Bioactive Materials 35 (2024) 429–444

Contents lists available at ScienceDirect

Bioactive Materials

journal homepage: www.keaipublishing.com/en/journals/bioactive-materials

Boosting cartilage repair with silk fibroin-DNA hydrogel-based cartilage organoid precursor

Congyi Shen [a,b,c,d,e,1], Jian Wang [a,b,c,e,f,1], Guangfeng Li [a,b,c,e,g,1], Shuyue Hao [a,b,c,d,e,1], Yan Wu [a,b,e], Peiran Song [a,b,e], Yafei Han [a,b,c,e], Mengmeng Li [a,b,e], Guangchao Wang [f], Ke Xu [a,b,e], Hao Zhang [a,b,e], Xiaoxiang Ren [a,b,e], Yingying Jing [a,b,e,**], Ru Yang [h,***], Zhen Geng [a,b,e,****], Jiacan Su [a,b,e,f,*]

[a] Institute of Translational Medicine, Shanghai University, Shanghai, 200444, China
[b] Organoid Research Center, Shanghai University, Shanghai, 200444, China
[c] School of Medicine, Shanghai University, Shanghai, 200444, China
[d] School of Life Sciences, Shanghai University, Shanghai, 200444, China
[e] National Center for Translational Medicine (Shanghai) SHU Branch, Shanghai University, Shanghai, 200444, China
[f] Department of Orthopedics, Xinhua Hospital, Shanghai Jiao Tong University School of Medicine, Shanghai, 200092, China
[g] Department of Orthopedics, Shanghai Zhongye Hospital, Shanghai, 200941, China
[h] Second Affiliated Hospital of Soochow University, Departments of Rheumatology and Immunology, Soochow, 215000, China

ARTICLE INFO

Keywords:
Silk fibroin-DNA hydrogel
Microsphere
Chondrogenesis
Cartilage organoid
Cartilage repair

ABSTRACT

Osteoarthritis (OA), a common degenerative disease, is characterized by high disability and imposes substantial economic impacts on individuals and society. Current clinical treatments remain inadequate for effectively managing OA. Organoids, miniature 3D tissue structures from directed differentiation of stem or progenitor cells, mimic native organ structures and functions. They are useful for drug testing and serve as active grafts for organ repair. However, organoid construction requires extracellular matrix-like 3D scaffolds for cellular growth. Hydrogel microspheres, with tunable physical and chemical properties, show promise in cartilage tissue engineering by replicating the natural microenvironment. Building on prior work on SF-DNA dual-network hydrogels for cartilage regeneration, we developed a novel RGD-SF-DNA hydrogel microsphere (RSD-MS) via a microfluidic system by integrating photopolymerization with self-assembly techniques and then modified with Pep-RGDfKA. The RSD-MSs exhibited uniform size, porous surface, and optimal swelling and degradation properties. *In vitro* studies demonstrated that RSD-MSs enhanced bone marrow mesenchymal stem cells (BMSCs) proliferation, adhesion, and chondrogenic differentiation. Transcriptomic analysis showed RSD-MSs induced chondrogenesis mainly through integrin-mediated adhesion pathways and glycosaminoglycan biosynthesis. Moreover, *in vivo* studies showed that seeding BMSCs onto RSD-MSs to create cartilage organoid precursors (COPs) significantly enhanced cartilage regeneration. In conclusion, RSD-MS was an ideal candidate for the construction and long-term cultivation of cartilage organoids, offering an innovative strategy and material choice for cartilage regeneration and tissue engineering.

1. Introduction

Osteoarthritis (OA) is a prevalent degenerative joint disease characterized by the degradation of joint cartilage, representing a primary cause of adult disability globally [1–3]. Statistics indicate that over five hundred million individuals worldwide suffer from OA, imposing significant societal and economic burdens [4,5]. Due to the avascular

Peer review under responsibility of KeAi Communications Co., Ltd.

* Corresponding authors. Institute of Translational Medicine, Shanghai University, Shanghai, 200444, China.
** Corresponding author. Institute of Translational Medicine, Shanghai University, Shanghai, 200444, China.
*** Corresponding author. Second Affiliated Hospital of Soochow University, Departments of Rheumatology and Immunology, Soochow, 215000, China.
**** Corresponding author. Institute of Translational Medicine, Shanghai University, Shanghai, 200444, China.
E-mail addresses: jingy4172@shu.edu.cn (Y. Jing), yangru923@126.com (R. Yang), nanboshan1987@163.com (Z. Geng), drsujiacan@163.com (J. Su).
[1] These authors contributed equally to this study.

https://doi.org/10.1016/j.bioactmat.2024.02.016
Received 2 January 2024; Received in revised form 12 February 2024; Accepted 14 February 2024

Abbreviations

OA	osteoarthritis
SF	silk fibroin
BMSCs	bone marrow mesenchymal stem cells
RGD	Arginine-Glycine-Aspartic Acid
SD-MS	SF-DNA hydrogel microsphere
RSD-MS	RGD-SF-DNA hydrogel microsphere
COP	cartilage organoid precursor
OAT	osteochondral autograft transplantation
ACI	autologous chondrocyte implantation
MACI	matrix-induced autologous chondrocyte implantation
ECM	extracellular matrix
ssDNA	single-stranded DNA
LAP	Lithium Phenyl-2,4,6-trimethylbenzoylphosphinate
NMR	nuclear magnetic resonance
SEM	scanning electron microscopy
PBS	phosphate buffered saline
GAG	glycosaminoglycan
Col II	collagen type II
ELISA	enzyme-linked immunosorbent assay
DMMB	1,9-dimethylmethylene blue
qRT-PCR	quantitative real-time PCR
Col I	collagen type I
Col X	collagen type X
ACAN	aggrecan
mRNA-seq	mRNA sequencing
PCA	principal component analysis
DEGs	differentially expressed genes
GO	gene ontology
KEGG	Kyoto encyclopedia of genes and genomes
GSEA	gene set enrichment analysis
ICRS	international cartilage repair society
AFM	atomic force microscopy
Ra	roughness parameter
H&E	hematoxylin and eosin
IHC	immunohistochemistry
CCK-8	Cell Counting Kit-8
ECL	enhanced chemiluminescence
IVIS	*in vivo* imaging system

nature of cartilage, coupled with its low cellular density and limited cell migration capacity, its intrinsic repair capabilities are significantly constrained. Current mainstream strategies for cartilage repair in clinical practice, including microfracture, osteochondral autograft transplantation (OAT), allogeneic cartilage transplantation, and implantation of processed allogeneic cartilage, while widely applied in clinical settings, all exhibit certain limitations and deficiencies [6–8]. For instance, microfracture may lead to inadequate defect filling and cartilage fibrosis [9,10]. OAT encounters issues related to donor site limitations and graft adaptation. Allogeneic cartilage transplantation presents risks of immune rejection and infection, with difficulties in matching allogeneic tissue to autologous cartilage possibly resulting in biomechanical imbalances and decreased joint load-bearing capacity [11]. Consequently, existing methods fail to provide a sustainable remedy for cartilage degeneration. In the interim, tissue engineering technologies for cartilage regeneration, such as autologous chondrocyte implantation (ACI) and matrix-induced autologous chondrocyte implantation (MACI), have introduced innovative strategies with notable effectiveness. Nevertheless, the current chondrocyte expansion strategies reliant on two-dimensional (2D) systems may induce cell dedifferentiation, highlighting the imperative for conducting three-dimensional (3D) cell culture *in vitro* to better preserve cell morphology, function, and the biomechanical integrity of grafts [12]. Hence, there is an urgent need for novel techniques and approaches to address the challenges in cartilage repair.

Organoids are self-renewing, and self-organizing 3D microstructures derived from directed differentiation of stem cells or progenitor cells, possessing critical characteristics, structure, and functions resembling certain aspects of organs [13,14]. This structure, to some extent, mimics organ functionality and is not only applicable for drug evaluation but also serves as an active transplant to facilitate the repair of damaged organs [15]. Therefore, cartilage organoids should exhibit a 3D architecture akin to native cartilage, encompassing an ECM rich in Type II collagen and proteoglycans, as well as embedded chondrocytes. Additionally, cartilage organoids could exhibit mechanical characteristics that closely resemble those of native cartilage, thereby facilitating the emulation of the intrinsic *in vivo* functionalities of natural cartilage. Moreover, they could be capable of integrating into host tissue, contributing to the repair and regeneration of damaged cartilage [16]. Thus, constructing cartilage organoids as an *in vitro* 3D research model or transplant material for cartilage regeneration presents a novel avenue for cartilage tissue engineering [17,18]. Besides, the construction of cartilage organoids necessitates a 3D network scaffold similar to the extracellular matrix (ECM) of cartilage to support the proliferation of chondrocyte and maintain their physiological functions [19,20]. Matrigel, a commercialized hydrogel widely used for organoid culture, offers an environment resembling the ECM [21]. However, the use of Matrigel has certain limitations in scientific research and clinical applications [22]. Firstly, as Matrigel is extracted from mouse sarcoma cultures, its animal-derived nature may limit its clinical applicability. Secondly, batch-to-batch variations of Matrigel may affect the consistency and reproducibility of experimental outcomes. Additionally, as a complex mixture, the composition of Matrigel is not fully defined, affecting its application specificity and predictability. Therefore, developing a hydrogel with better controllability, customizability, and a clear composition for constructing organoids is crucial for advancing regenerative medicine and tissue engineering [23].

DNA hydrogel formed by the self-assembly of DNA strands into a 3D network [24,25]. They retain the favorable biocompatibility, biodegradability, and programmability of DNA and seamlessly integrate with the mechanical properties of their framework, making them an ideal material for constructing cartilage organoids. In comparison to pure DNA hydrogels, hybrid DNA hydrogels exhibit superior mechanical performance [26,27]. In our previous research, we successfully developed a hybrid silk fibroin-DNA (SF-DNA) hydrogel with tunable surface rigidity [28]. In this hydrogel, a supramolecular network formed through DNA base pairing induces the development of β-sheet structures by constraining and aggregating SF molecules. By adjusting the ratio of DNA to SF, chondrogenic differentiation of bone marrow mesenchymal stem cells (BMSCs) can be facilitated. RGD, a short peptide sequence composed of three amino acids, serves as a specific ligand for integrins on cell membranes and finds wide application in the field of biomaterials [29]. Modifying hydrogels with RGD can provide a platform that mimics the natural cartilage microenvironment, promoting cell adhesion, proliferation, and chondrogenic differentiation. Hydrogel microspheres modified with RGD can enhance the effective payload of BMSCs, thus unleashing greater potential in regenerative medicine and tissue engineering [30].

In this study, building upon our previous research on the SF-DNA double network hydrogel that promotes cartilage regeneration, we developed RGD-SF-DNA hydrogel microspheres (RSD-MSs) capable of loading BMSCs (Scheme 1). In the preparation process, we initially utilized microfluidic technology, combining silk methacrylate (SilMA) and supramolecular DNA hydrogel techniques to fabricate SF-DNA

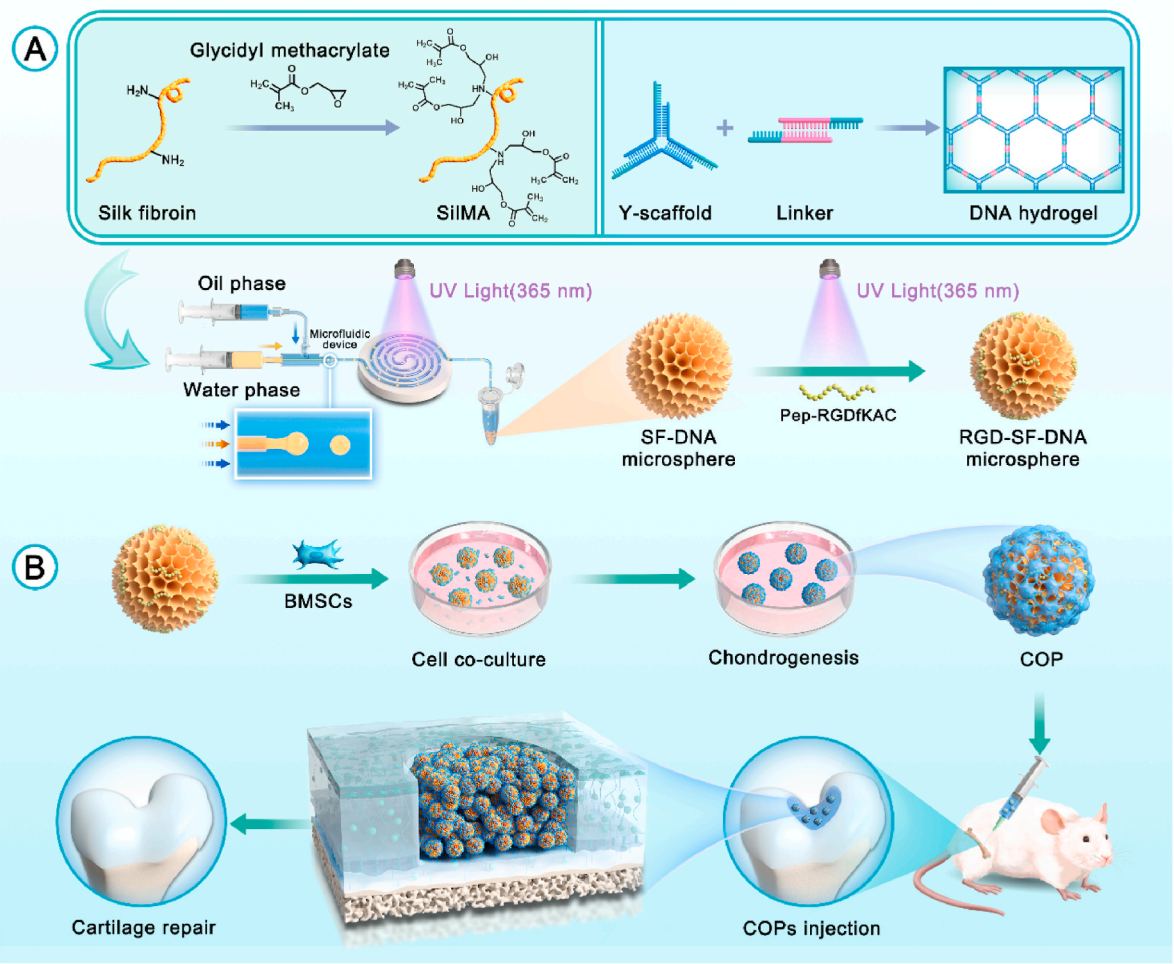

Scheme 1. Schematic diagram of (A) the synthesis of RGD-SF-DNA microspheres and (B) their application in the preparation of cartilage organoid precursors (COPs) and cartilage regeneration.

double network hydrogel microspheres (SD-MSs). Subsequently, these hydrogel microspheres were surface-modified using photo-polymerization with Pep-RGDfKA. The modified RSD-MSs demonstrated excellent biocompatibility, bioadhesiveness, and the ability to promote chondrogenic differentiation. Furthermore, BMSCs were seeded onto these RSD-MSs for *in vitro* chondrogenic induction experiments, leading to the creation of cartilage organoid precursors (COPs). In *in vivo* studies, COPs significantly enhanced cartilage regeneration. In summary, we proposed that RSD-MS served an ideal candidate for the construction and long-term cultivation of cartilage organoids, providing an innovative strategy and material choice for cartilage regeneration and tissue engineering.

2. Results

2.1. Synthesis and characterization of RSD-MSs

In this study, we initially dissolved and mixed single-stranded DNA (ssDNA), SilMA, and the photoinitiator Lithium Phenyl-2,4,6-trimethylbenzoylphosphinate (LAP) to prepare a precursor mixture for SF-DNA. SilMA is a derivative formed by introducing methacrylate groups onto the amine residues of SF. The construction of the DNA hydrogel is based on two components: Y-scaffold and L-Linker. After complete mixing of the ssDNA solution, Y-ssDNA and L-ssDNA rapidly form physical crosslinks through base pairing, creating the first DNA supramolecular network. This DNA supramolecular network exhibits excellent injectability and self-healing properties, suitable for subsequent microsphere fabrication.

During the microspheres fabrication, we employed microfluidic technology, a method for precise control and manipulation of fluids, combined with photo-crosslinking to produce SF-DNA dual-network hydrogel microspheres. The microfluidic coaxial needle used comprised two concentric needles, with the inner needle delivering the aqueous phase (SF-DNA precursor mixture) and the outer needle delivering the oil phase. Microsphere formation relies on the shear force generated by the oil phase, encapsulating the aqueous droplets within the oil, forming uniformly sized microspheres. By adjusting the flow rate ratio of the oil and aqueous phases, the size of the microspheres can be precisely controlled. Under UV light at 365 nm, the SF-DNA precursor droplets undergo crosslinking, forming the second network of SF, thus yielding SD-MSs. Pep-RGDfKAC, a peptide sequence of Arginine-Glycine-Aspartic Acid (RGD) with an acryloyl group, is used for surface modification of the SD-MSs, resulting in RSD-MS.

Microscopic images of demonstrated that both SD-MSs and RSD-MSs exhibited good dispersibility, size uniformity, and intact shape (Fig. 1A). Particle size distribution revealed that the average diameter of SD-MS was 545.2 ± 27.8 μm, while RSD-MS averaged 527.5 ± 25.55 μm (Fig. 1B). In nuclear magnetic resonance (NMR) hydrogen spectrum analysis, the characteristic signal of methyl groups in alanine is typically observed at 1.2 ppm. Correspondingly, in the NMR spectrum of RSD-MSs, a new peak emerged at 1.2 ppm, indicating successful modification of Pep-RGDfKA onto SD-MSs (Fig. 1C). Cold field emission scanning electron microscopy (SEM) observations of SD-MS and RSD-MS showed uniformly porous surfaces for both (Fig. 1D and E). The pore size of

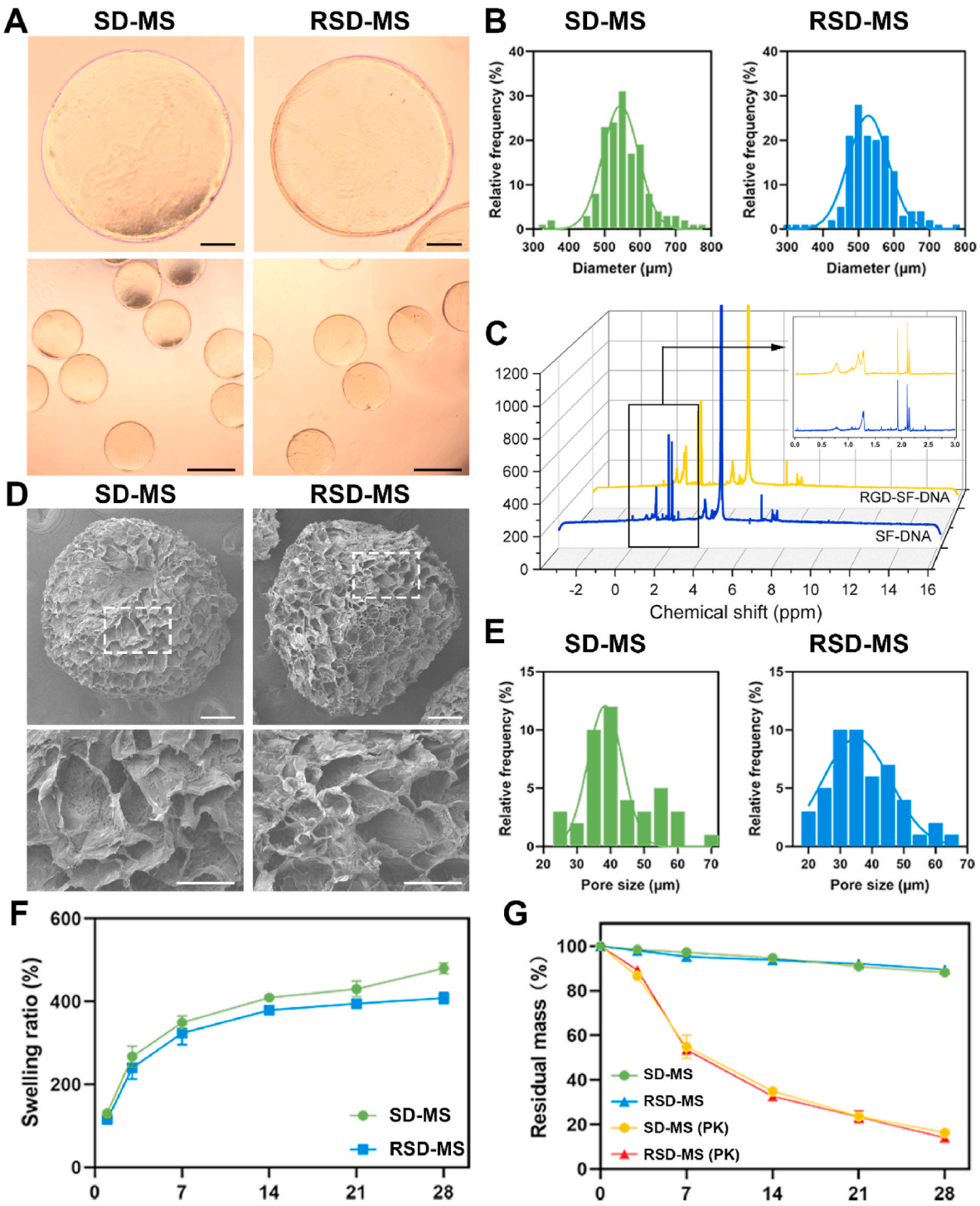

Fig. 1. Synthesis and characterization of RSD-MS. (A) Microscopic images of SD-MS and RSD-MS. (B) Particle size distribution of SD-MSs and RSD-MSs. The lower sections display lower magnification images (scale bars: 500 μm) in the upper sections (scale bars 100 μm). (C) 1H NMR spectrogram of SD-MSs and RSD-MSs. (D) SEM images of SD-MS and RSD-MS. The lower sections display higher magnification sections (scale bars: 50 μm) of the areas highlighted by white boxes in the upper panels (scale bars 100 μm). (E) Pore size of SD-MSs and RSD-MSs. (F) The swelling ratio of SD-MSs and RSD-MSs in PBS at 37 °C. (G) *In vitro* degradation curves of SD-MSs and RSD-MSs in PBS and protease K solution at 37 °C.

SDMS was 38.4 ± 12.08 μm, while RSD-MS had a pore size of 35.1 ± 9.3 μm. These porous structures facilitate cell migration and adhesion, with minimal impact of Pep-RGDfKAC modification on pore size. Furthermore, we evaluated the swelling behavior of SD-MSs and RSD-MSs in phosphate buffered saline (PBS) (Fig. 1F). Results showed that SD-MSs and RSD-MSs reached swelling rates of 349.1 ± 16.0% and 323.6 ± 18.3%, respectively, in the first week, gradually increasing to 480 ± 12% and 408 ± 15% by the fourth week. RSD-MSs exhibited slightly lower swelling compared to SD-MS, likely due to its smaller porosity. Cell migration, differentiation, and ECM synthesis in hydrogels are influenced by swelling characteristics [31]. Appropriate swelling provides the necessary physical and chemical environment for BMSCs growth and differentiation. These findings suggested that SD-MSs and RSD-MSs have good structural stability and appropriate swelling rates,

supporting their use in long-term construction of cartilage organoids. Hydrogel degradation characteristics play a crucial role in constructing cartilage organoids. Inappropriate degradation rates, either too fast or too slow, can hinder the regeneration process. Proper degradation of porous hydrogel microspheres is vital for maintaining the survival and function of loaded cells. To simulate *in vivo* degradation, we conducted experiments in a protease K-rich environment. By monitoring the residual mass of SD-MSs and RSD-MSs in PBS and protease K solution, we studied their degradation patterns. After 28 days of degradation in PBS environment, both SD-MSs and RSD-MSs showed limited degradation, indicating high structural stability (Fig. 1G). However, in the protease K environment, the residual mass of both microspheres gradually decreased over time, with no significant difference between them. The mass reduced from 55.2 ± 3.9% in the first week to 13.9 ± 0.4% in the fourth week. The scaffold degradation rate should balance with ECM deposition induced by stem cells. Too rapid degradation could lead to larger porosity, reducing ECM deposition, while a controlled degradation rate facilitates cell proliferation and ECM formation, enhancing cell permeation and intercellular interactions [32]. These results indicated that SD-MSs and RSD-MSs have suitable structural stability and degradation rates, likely benefiting ECM deposition and providing favorable conditions for constructing cartilage organoids.

2.2. Biocompatibility and cell adhesion of RSD-MS

To comprehensively evaluate the *in vitro* cellular compatibility of SD-MSs and RSD-MSs, we employed a transwell coculture system for BMSCs and hydrogel microspheres. Live/dead cell staining conducted on days 1, 3, and 5 of culture indicated high BMSCs viability (green fluorescence) in both SD-MS and RSD-MS groups, with almost no dead cells (red fluorescence), similar to the control group. This demonstrated the non-cytotoxicity of SD-MSs and RSD-MSs (Fig. 2A and S1A, B). CCK-8 assay results showed significant proliferation of BMSCs in both SD-MS and RSD-MS groups from day 1 to day 5, with no statistically significant differences between time points (Fig. 2B), further proving their good cellular compatibility. To explore RSD-MSs' ability to promote cell adhesion, and proliferation, we cocultured BMSCs with RSD-MSs (Fig. 2C). Cell enumeration on each microsphere was conducted, and the results indicated that, over time, cell adhesion and proliferation on RSD-MS were significantly enhanced in comparison to the SD-MS group. The quantity of cells on the microspheres increased from 29 ± 5 on day 1–112 ± 10 on day 3, eventually reaching 332 ± 31 by day 7 (Fig. 2D). Consistently, CCK-8 assay outcomes corroborated these findings, suggesting that the incorporation of RGD significantly augmented the microspheres' cell adhesion capacity (Fig. S2). We performed cytoskeletal and nuclear staining on cells on RSD-MSs. Staining results showed that on day 1 of culture, cells had successfully adhered to the microspheres, with some maintaining a round shape while others began to spread their pseudopodia. By day 3, almost all cells had spread their pseudopodia, and cell morphology became more elongated, displaying typical spindle-shaped or polygonal shapes, with a marked augmentation in cell number. By day 7, BMSCs covered the entire microsphere, even beginning to infiltrate inside. Notably, by day 14, microspheres filled with cells started to adhere to each other and aggregate into micro-tissues (Fig. 2E). RSD-MS, as a microscaffold for cell growth, with its larger specific surface area, enhanced cell spreading and intercellular interactions, promoting the proliferation of attached cells. These results indicated that RSD-MSs provide an excellent microenvironment for cells, supporting cell adhesion, proliferation, and infiltration, thus benefiting the construction of cartilage organoids.

2.3. RSD-MS promote chondrogenic differentiation of BMSCs

After characterizing the cellular compatibility and adhesion of SD-MSs and RSD-MSs, we further explored their influence on BMSCs chondrogenic differentiation. Subsequently, COPs were constructed by subjecting RSD-MS loaded with BMSCs to chondrogenic induction for a period of 14 days. To promote cartilage tissue formation, chondrogenic induction experiments were conducted in wells containing SD-MS and RSD-MS, and glycosaminoglycan (GAG) content related to

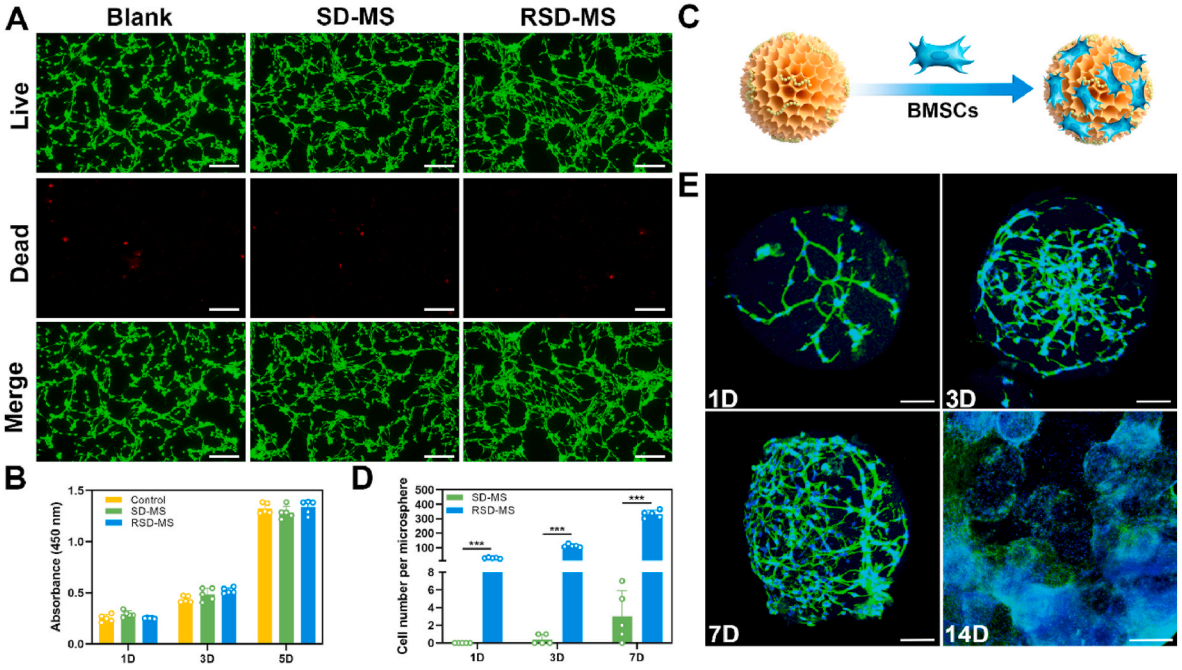

Fig. 2. Biocompatibility and cell adhesion of microspheres. (A) Live/dead staining images of BMSCs cocultured with blank, SD-MSs and RSD-MSs for 5 days (scale bars 100 μm). (B) BMSCs proliferation cocultured with blank, SD-MS and RSD-MS for 1, 3 and 5 days. (C) Schematic representation of BMSCs loaded with microspheres. (D) Number of BMSCs cocultured with SD-MS and RSD-MS for 1, 3, and 7 days. (E) Phalloidin-stained and Dapi-stained BMSCs cocultured with RSD-MS for 1, 3, 7 days imaged via confocal laser scanning microscopy (scale bars 100 μm). And phalloidin-stained and Dapi-stained BMSCs cocultured with RSD-MS for 14 days imaged via fluorescence microscope (scale bars 500 μm).

chondrogenesis was detected using Alcian Blue staining. We performed microscopic observation and quantitative analysis of Alizarin Blue staining in BMSCs cocultured with microspheres for 3, 7, and 14 days (Fig. 3A and B). On day 3, staining intensity differences among the three groups were not significant. By day 7, both SD-MS and RSD-MS groups showed significantly enhanced staining intensity compared to the blank group. On day 14, the RSD-MS group had the strongest staining intensity, followed by the SD-MS group, and the weakest in the blank group, indicating the highest GAG production in RSD-MS. Quantitative analysis suggested that RSD-MSs had a significantly higher impact on BMSCs chondrogenesis compared to SD-MSs, possibly due to RSD-MSs' higher cell adhesiveness providing more space and support for BMSCs growth. This 3D structure better mimicked the cartilage tissue microenvironment, facilitating BMSCs growth and differentiation.

To investigate the different hydrogel microspheres' effects on BMSCs chondrogenesis, we quantitatively assessed collagen type II (Col II) and GAG content in SD-MS and RSD-MS groups using enzyme-linked immunosorbent assay (ELISA) and 1,9-dimethylmethylene blue (DMMB) assay. The content of Col II and GAG in the RSD-MS group continuously increased over time, reaching the highest values on day 14, significantly higher than in the SD-MS group (Fig. 3C and D). These results further emphasized RSD-MSs' potential advantages in promoting BMSCs differentiation into chondrocytes. Subsequently, we used quantitative real-time PCR (qRT-PCR) to comparatively analyze the chondrogenic differentiation of BMSCs in different microsphere groups. We focused on analyzing genes related to fibrosis (Collagen Type I, Col I), hypertrophy (Collagen Type X, Col X), and cartilage-specific genes (Col II, Sox9, and Aggrecan, ACAN) (Fig. 3E–I). Compared to the SD-MS group, the RSD-MS group showed lower expression of Col I and Col X, and higher expression of Col II and ACAN on days 7 and 14. This indicated that RSD-MSs effectively promoted cartilage-specific gene expression and inhibits the development of fibrocartilage and calcified cartilage. Further validation was performed on RSD-MSs induced for 14 days, which are the COPs we constructed, using immunofluorescence staining. This confirmed the expression of Col II, Sox9, and ACAN, aligning with the results obtained from qRT-PCR (Fig. 3J). Additionally, from the immunofluorescence staining images, it can be observed that cells already covering the surface of the microspheres are growing inward into the RSD-MS. Finally, the expression of Col II, Sox9, and ACAN proteins was detected using Western Blot after 14 days of chondrogenic induction in each group. Compared to the blank group, the expression of Col II, Sox9, and ACAN was marked increased in both SD-MS and RSD-MS groups (Fig. 3K, **L** and **S3**). These results indicated that while both SD-MS and RSD-MS groups showed some induction capability, the induction effect of the RSD-MS group was notably superior to SD-MS, making it more suitable as a microscaffold for cultivating cartilage organoids.

2.4. Transcriptomic analysis of BMSCs on RSD-MS

To delve into the biological impact of RSD-MSs on BMSCs, this study employed mRNA sequencing (mRNA-seq) analysis. Principal component analysis (PCA) was utilized to compare gene expression patterns between control and RSD-MS groups (Fig. 4A). In PCA plots, the proximity of samples within a group indicates high reproducibility, while distances between groups reveal significant differences in gene expression. Comprehensive analysis revealed 3454 differentially expressed genes (DEGs), including 1945 downregulated and 1509 upregulated genes (Fig. 4B). Further analysis employed volcano plots and cluster heatmaps to display DEGs in each group (Fig. 4C and D).

Gene ontology (GO) analysis categorized DEGs across three aspects: biological processes, cellular components, and molecular functions. Compared to the blank, RSD-MS-treated BMSCs exhibited upregulation of genes positively regulating chondrocyte differentiation, collagen synthesis, and cell proliferation at the biological process level. At the molecular function level, genes associated with cell adhesion (such as collagen binding, integrin binding, ECM binding) and cytokine activity in the RSD-MS group showed an upward trend (Fig. 4E). Additionally, Kyoto encyclopedia of genes and genomes (KEGG) pathway enrichment analysis further revealed the functions of DEGs (Fig. 4F). The analysis corroborated previous findings, indicating upregulation of focal adhesion and ECM-receptor interaction in RSD-MS group, pathways crucial for cell-matrix interactions in chondrogenesis and regeneration. Notably, RSD-MSs also upregulated GAG biosynthesis-chondroitin sulfate/dermatan sulfate, calcium signaling pathway, and multiple pathways related to chondrogenesis. Besides, gene set enrichment analysis (GSEA) and pathway gene heatmaps suggested that RSD-MSs influence GAG biosynthesis by modulating integrin-mediated cell adhesion and focal adhesion, compared to the control group (Fig. 4G–I and Figs. S4A–C). The results of GO analysis, KEGG analysis, and GSEA collectively indicated that RSD-MSs significantly upregulates genes related to cell adhesion and chondral matrix synthesis, thereby enhancing the efficiency of BMSCs differentiation into chondrocytes and promoting chondral matrix synthesis, crucial for cartilage regeneration and the construction of cartilage organoids.

In summary, RSD-MSs provided a simulated cartilage growth microenvironment for BMSCs, particularly by upregulating integrin-mediated cell adhesion and focal adhesion pathways related to chondrogenesis-promoting signals. This upregulation promoted GAG biosynthesis, thereby enhancing the chondrogenic differentiation of BMSCs.

2.5. In Vivo evaluation of cartilage repair by RSD-MS

To assess the capacity of BMSCs-loaded RSD-MS in cartilage regeneration *in vivo*, a rat articular cartilage defect model (2 × 1.5 mm) was utilized in this study. Fig. 5A depicted experimental animals were randomly allocated to four different groups: Sham group (serving as the positive control), Control group (untreated experimental group), RSD-MS group (group treated solely with RSD-MSs), and COP group (group treated with COPs). Throughout the experimental procedure, at post-operative weeks 5 and 10, rats underwent euthanasia, following which tissue specimens from the femur, heart, liver, kidney, lung, and spleen were harvested for subsequent laboratory analyses [33].

Gross examination of the full-thickness cartilage tissue at the distal femur was conducted (Fig. 5B). Compared to the Control and RSD-MS groups, the cartilage regeneration tissue in the COP group exhibited good filling, smooth surface, and less adjacent cartilage degeneration, closely resembling normal cartilage. Further, macroscopic assessment was performed according to the standards of the International Cartilage Repair Society (ICRS) (Fig. 5C and S5A). The results revealed poor cartilage regeneration in the untreated Control group. In contrast, treatment with COPs significantly improved repair outcomes compared to the Control and RSD-MS groups. The Sham group maintained stable ICRS scores at different time points. The ICRS scores for the Control, RSD-MS, and COP groups showed an increasing trend over time, reaching their peak at week 10. Additionally, to assess the surface roughness of the treated area, atomic force microscopy (AFM) analysis was performed at week 10 to determine the surface roughness parameter (Ra) (Fig. 5D and E). The results indicated that the Ra value of the COP group, though slightly higher than the sham group, was markedly lower than the control and RSD-MS groups. This indicated that the surface smoothness of the regenerated cartilage in the COP group was similar to the sham group, suggesting the effectiveness of COP in promoting regeneration closer to normal cartilage.

To quantitatively evaluate the quality of tissue repair, this study employed Hematoxylin and Eosin (H&E) staining, Safranin O/Fast Green staining, and immunohistochemistry (IHC) for Col II and ACAN. H&E and Safranin O/Fast Green staining results at week 5 revealed significant knee cartilage damage in the control group, with repair tissue primarily fibrous, disorganized, and infiltrated by inflammatory cells. The cartilage layer structure was disrupted, and cell distribution was

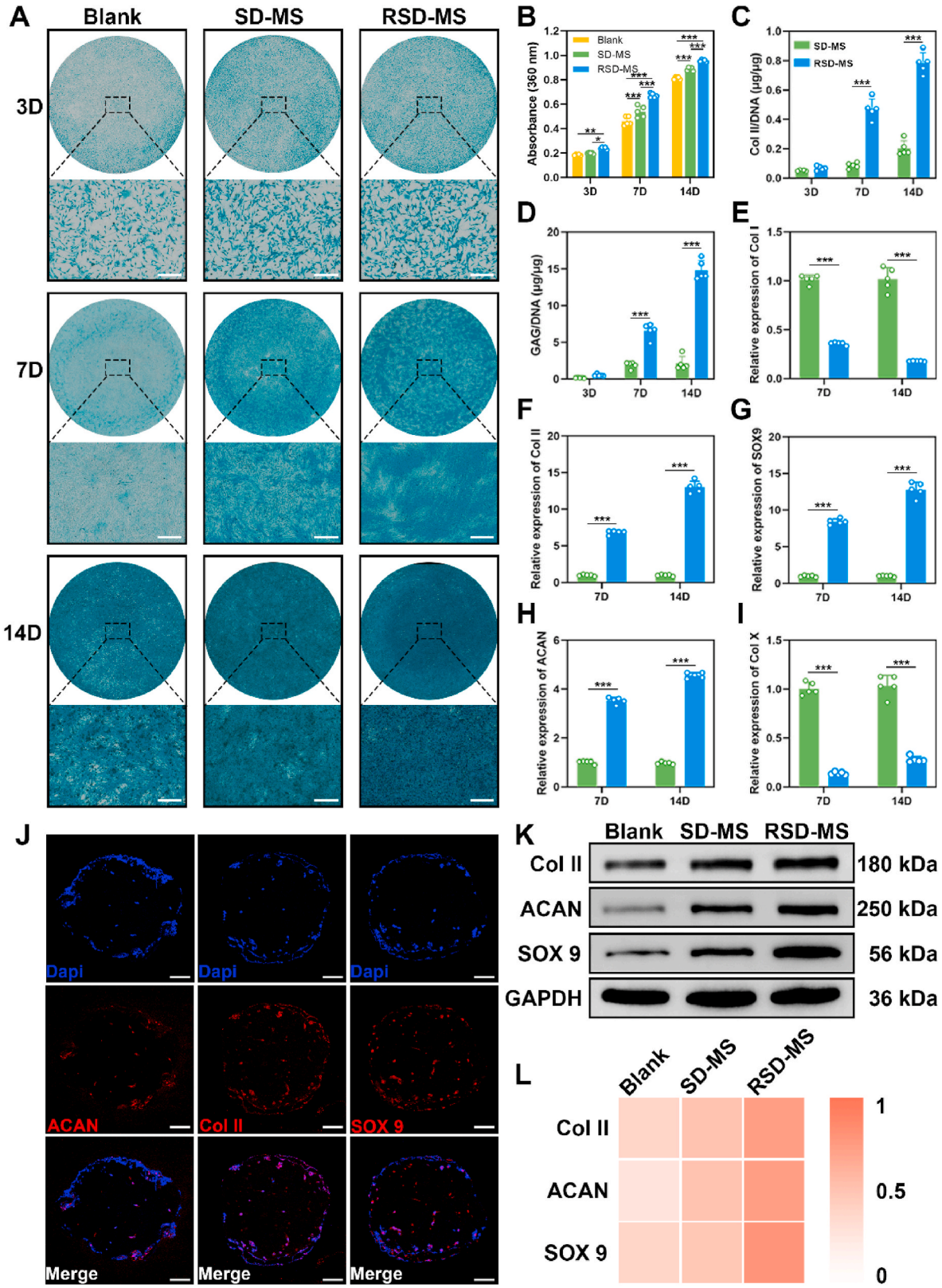

Fig. 3. The effect of SD-MSs and RSD-MSs on BMSCs chondrogenic differentiation. (A) Alcian staining of the BMSCs cultured with SD-MSs and RSD-MSs (transwell) for 3, 7, and 14 days (scale bars 200 μm). (B) Quantification of Alcian blue staining. (C and D) Relative production of GAG and Col II for BMSCs cultured on SD-MSs and RSD-MSs at 3, 7, and 14 days. (E–I) *In vitro* expression of Col I, Col II, SOX9, ACAN, and Col X) in BMSCs cocultured with blank, SD-MSs and RSD-MSs for 7, and 14 days. (J) Immunofluorescence images of Col II, SOX9 and ACAN on BMSCs loaded on RSD-MSs after 14 days of induction (scale bars 100 μm). (K) Representative Western blot results of Col II, SOX9 and ACAN. (L) Quantitative analysis of Western blot.

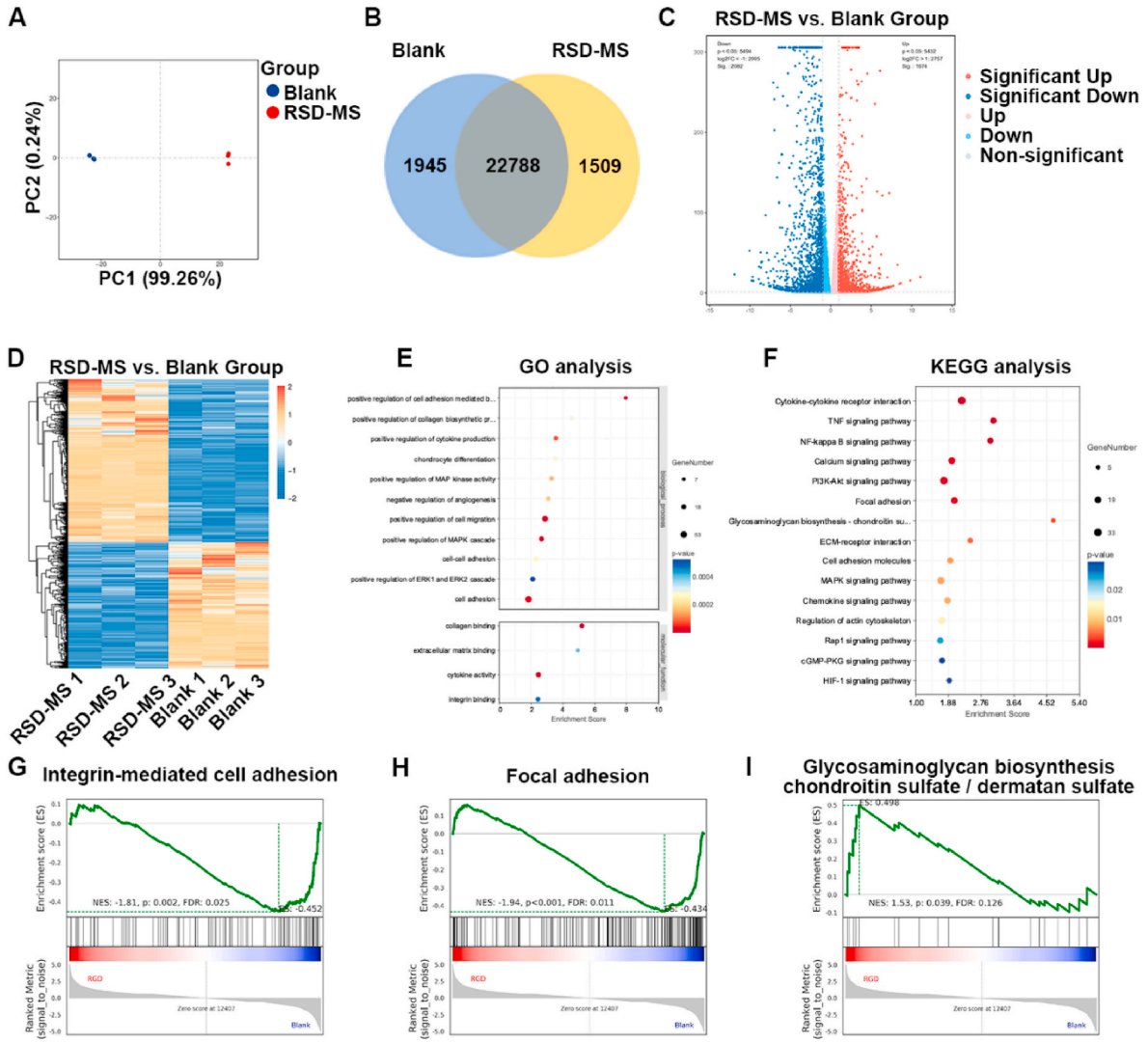

Fig. 4. Transcriptomic analysis. (A) PCA of DEGs distributed in the blank group and RSD-MS group. (B) Comparative assessment of mRNA expression in the blank group and RSD-MS group. (C) Volcano plot representation of genes exhibiting significant expression changes exceeding a 2-fold difference in transcriptome sequencing results. (D) Heatmap of gene expression clustering for DEGs. (E) GO analysis for upregulated genes in BMSCs. (F) KEGG analysis for upregulated genes in BMSCs. (G–I) GSEA enrichment analysis for integrin-mediated cell adhesion pathway, focal adhesion pathway and glycosaminoglycan biosynthesis-chondroitin sulfate/dermatan sulfate in BMSCs.

uneven. By week 10, further disorganization of the cartilage layer structure was observed, with a significant reduction in cell density and almost no cartilage matrix remodeling, accompanied by gradual degeneration of adjacent cartilage. In contrast, the RSD-MS group at week 5 showed filling and regenerative tissue in the cartilage defect area but with an irregular surface and uneven matrix staining. By week 10, the regenerative cartilage surface in this group was uneven, and the matrix was thin and uneven. The COP group at week 5 displayed complete regenerative cartilage structures, uniform cell distribution, and with time, an increase in staining and thickness of the repair tissue. By week 10, the regenerative cartilage surface in the COP group showed a smoothness similar to the sham group, with a uniform but slightly thin matrix (Fig. 6A and B). The O'Driscoll scoring system was utilized to quantitatively measure the degree and quality of cartilage repair. Results indicated that the COP group had significantly higher scores at all time points compared to the control and RSD-MS groups, with histological scores at week 10 approaching those of the sham group (Fig. S5B). IHC staining and semi-quantitative analysis showed that, consistent with Safranin O/Fast Green staining results, the COP group had significantly higher levels of ACAN and Col II expression at all time points compared to the control and RSD-MS groups, suggesting better cartilage repair quality in the COP group without hypertrophic cartilage remodeling (Fig. 7A–D).

Additionally, the *in vivo* cytotoxicity of the implanted materials was assessed. Routine blood analysis and liver and kidney function tests indicated no apparent systemic toxicity in all groups (Fig. 8A). H&E staining results showed that the main organ structures of rats in all groups were basically normal at 5 and 10 weeks post-operation (Fig. 8B), indicating that the use of these microspheres in rats are safe. To explore the *in vivo* biodegradation behavior of RSD-MSs, this study conducted *in vivo* degradation experiments by injecting fluorescently labeled RSD-MSs into the rat joint cavity (Fig. 8C). Results displayed in Fig. 8D elucidate the temporal degradation profile of RSD-MSs, affirming their favorable biodegradability. Notably, at the three-week mark, the fluorescence emanating from RSD-MSs was markedly diminished, suggesting significant material breakdown. This degradation process was more pronounced by the fourth week, where the fluorescence signal was virtually undetectable, indicating near-complete dissolution of the microspheres. By the fifth week, the complete *in vivo* degradation of RSD-MS was observed, corroborating the histological evidence provided by

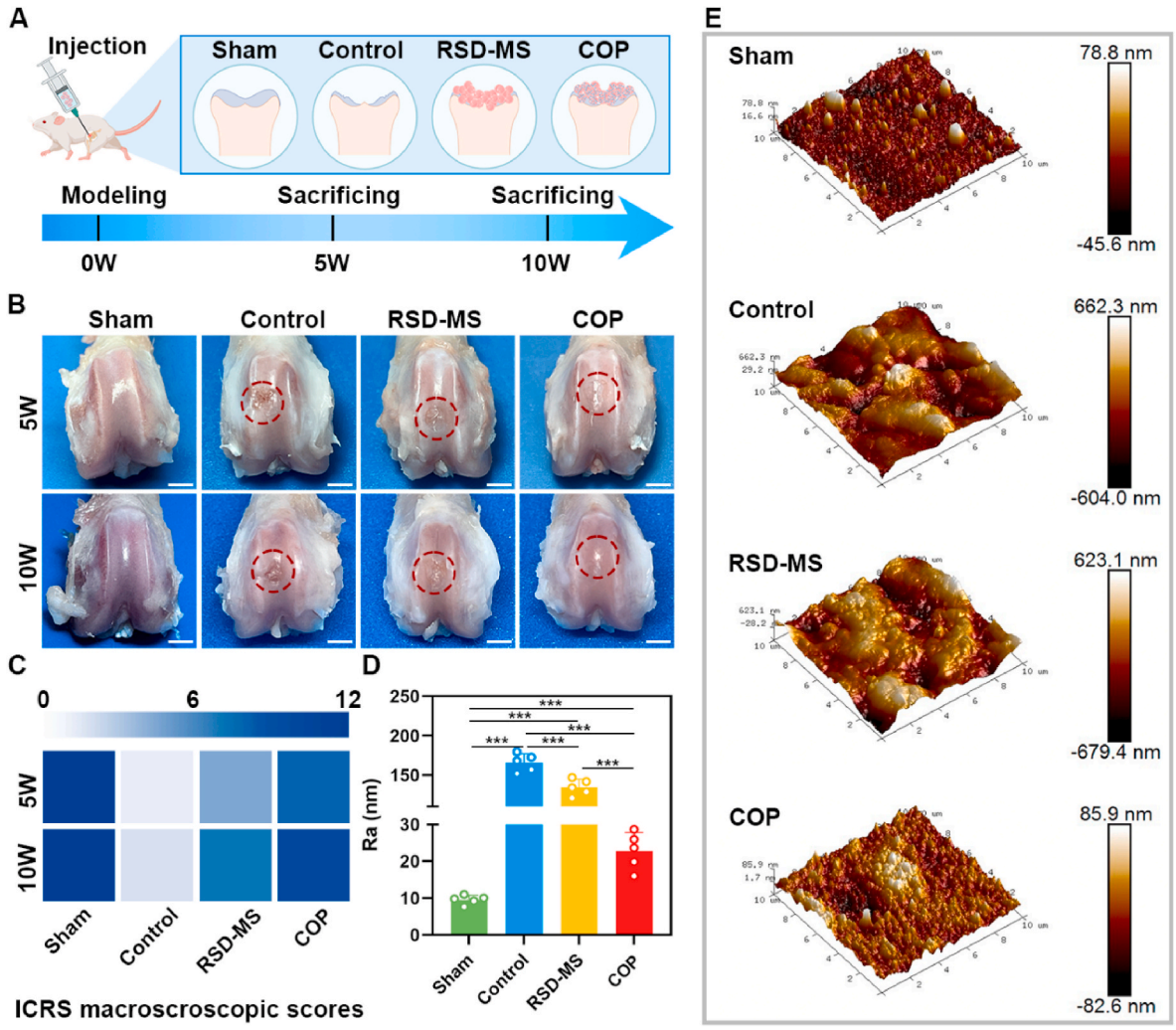

Fig. 5. (A) Scheme of cartilage defect modeling and treatment protocol. (B) Gross observation of femur cartilage after treatment at 5 and 10 weeks (scale bars 2 mm). (C) Heat map of ICRS macroscopic assessment of cartilage at 5 and 10 weeks. (D) Roughness parameter of the cartilage surface regeneration zone at10 weeks after treatment. (E) The AFM images of the cartilage surface regeneration zone at10 weeks after treatment (10 × 10 mm).

H&E staining. This sequential degradation underscores the potential of RSD-MSs as an efficient and biocompatible material for biomedical applications. The appropriate degradation rate not only promoted cartilage regeneration but also indicated that RSD-MS has a strong stability, making it an ideal material to support long-term cultivation of cartilage organoids.

The comprehensive results indicated that RSD-MS effectively facilitates the *in vivo* loading of BMSCs, enabling COPs to promote the secretion of cartilage-related ECM by cells, thus achieving rapid and effective cartilage repair. These findings provided vital experimental evidence for cartilage repair and regenerative medicine.

3. Discussions

Developing cartilage organoids is a critical breakthrough in regenerative medicine and tissue engineering [34,35]. This involves using tissue engineering techniques to construct micro-cartilaginous tissues, aiming to emulate the function and structure of natural cartilage. The main objective of this technology is to treat cartilage injuries or diseases, such as OA, sports injuries, or congenital defects [16,36]. Although Matrigel is the most commonly used product in organ-like ECM construction, its limitations in building cartilage organoids include batch variability, unclear composition, and lack of customization. Therefore, developing biomaterials as Matrigel alternatives for cartilage organoid construction is crucial. Recent studies have explored different materials for this purpose. For instance, Xing et al. used hyaluronic acid and gelatin to create microspheres for in situ self-assembled cartilage organoid construction, repairing canine cartilage defects [37]. Similarly, Lin et al. utilized gelatin-based microspheres loaded with MSCs for 3D self-assembly, repairing rabbit cartilage defects [38]. Additionally, Yin et al. employed polylactic acid and poly-L-glutamic acid/dehydrogenase hydrogels to construct columnar cartilaginous microtissues for rabbit cartilage repair [39].

As a novel biomaterial, DNA hydrogel exhibits excellent biocompatibility, biodegradability, and a 3D structural network [40]. This hydrogel has shown unique potential in the construction of cartilage organoids. Its physical and chemical properties can be precisely controlled by adjusting DNA sequences, lengths, or crosslinking patterns, making it applicable in cartilage tissue engineering where highly customized structures are needed. However, pure DNA hydrogels have limitations in cartilage repair applications due to their lower mechanical strength. E. Krieg and colleagues developed a DNA-poly (acrylamide-co-acrylic acid) hybrid hydrogel for culturing various organoids, such as human mesenchymal stromal cells-based organoids, pluripotent stem cells-based organoids, canine kidney cyst organoids, and human trophoblast organoids [41]. This DNA hybrid hydrogel supports organoid cultures for up to three weeks. Therefore, developing DNA hybrid hydrogels with a mechanically supportive framework can overcome the

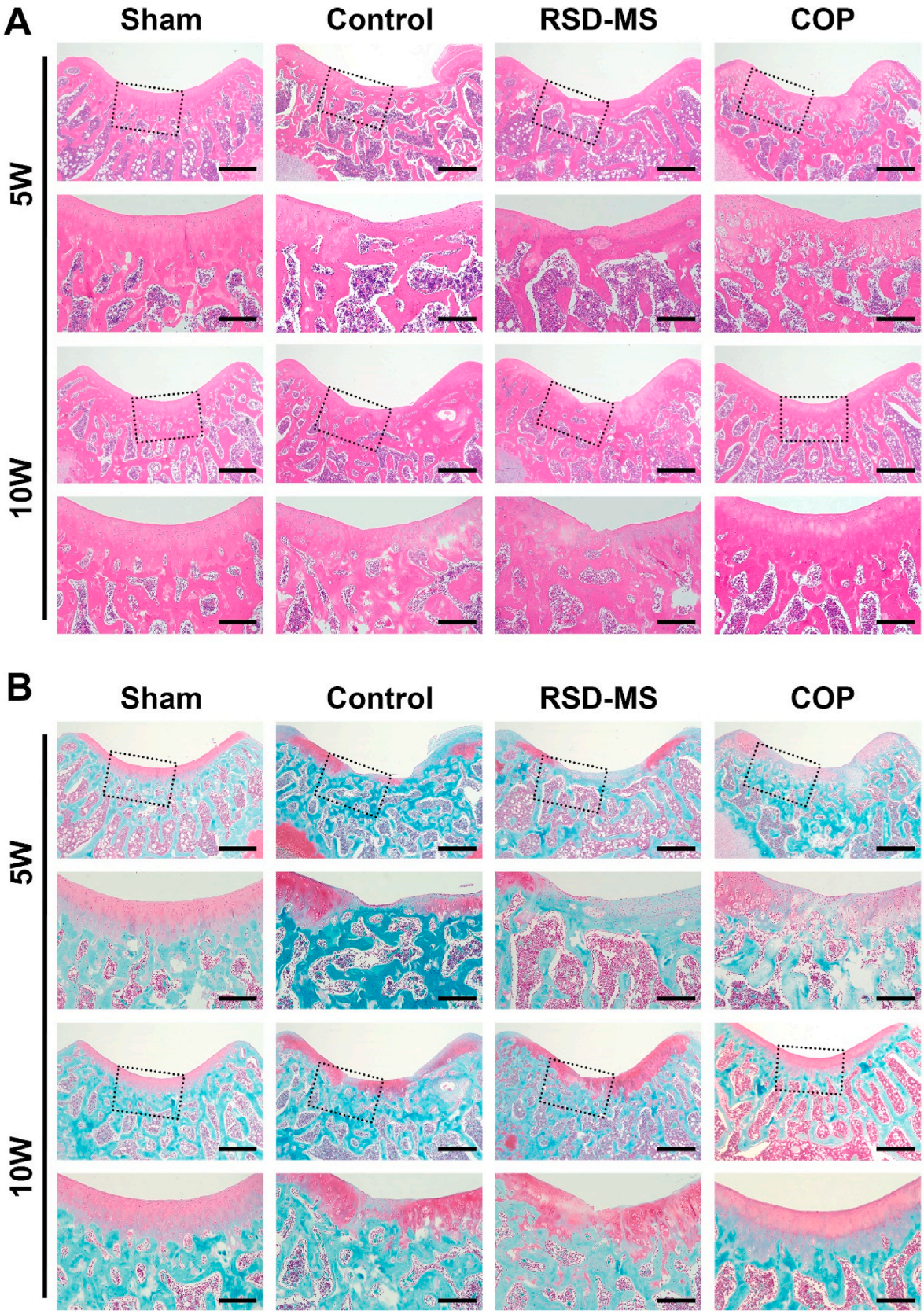

Fig. 6. (A) Representative H&E staining of femur cartilage at 5 and 10 weeks after treatment. Scale bars, 500 μm and 200 μm. (B)Representative Safranin O/Fast Green staining of femur cartilage at 5 and 10 weeks after treatment. Scale bars, 500 μm and 200 μm.

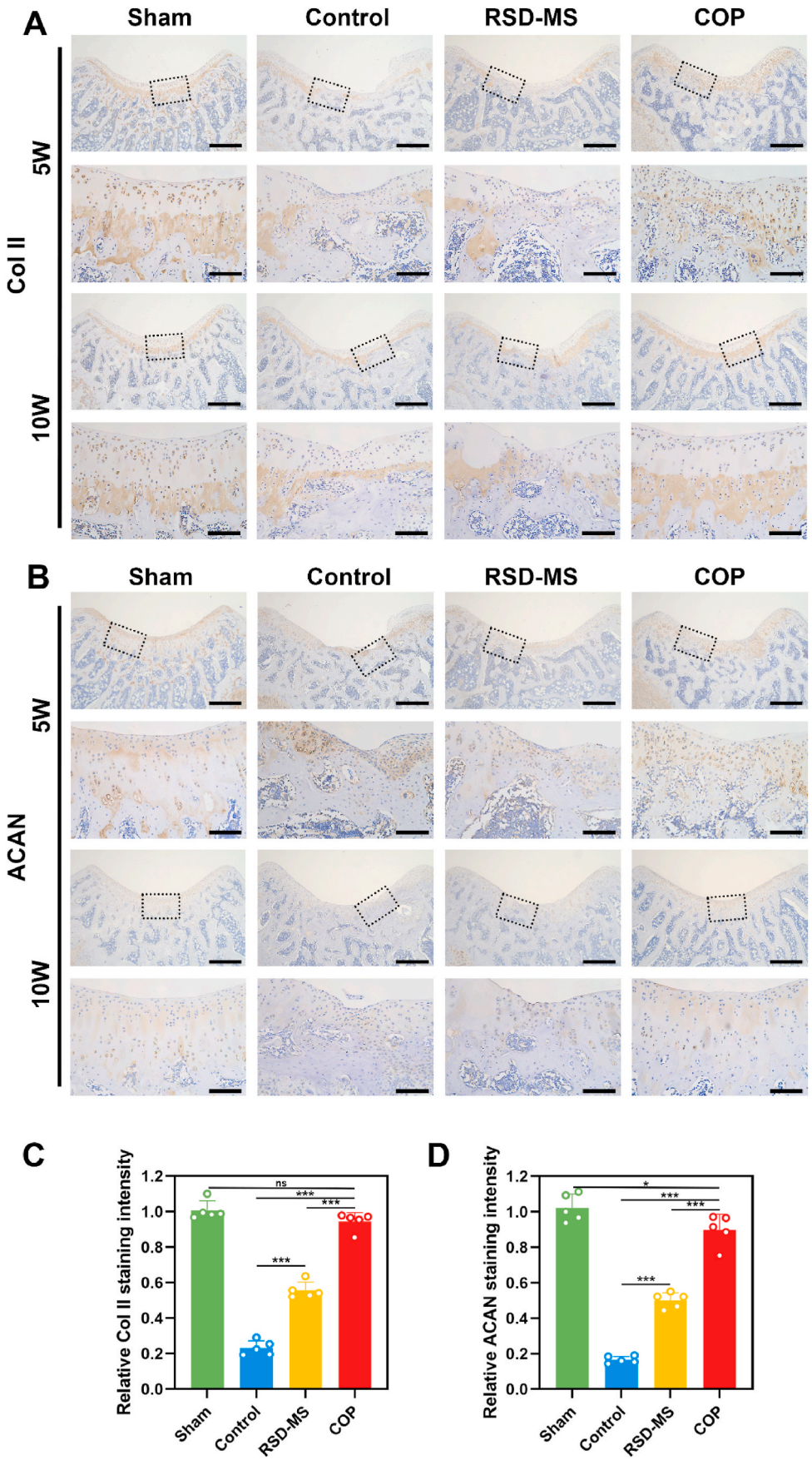

Fig. 7. (A)Immunohistochemical staining of Col II in rat cartilage post-treatment defects. Scale bars, 500 μm and 100 μm. (B)Immunohistochemical staining of ACAN in rat cartilage post-treatment defects. Scale bars, 500 μm and 100 μm. (C) Quantitative analysis of the Col II content. (D) Quantitative analysis of the ACAN content.

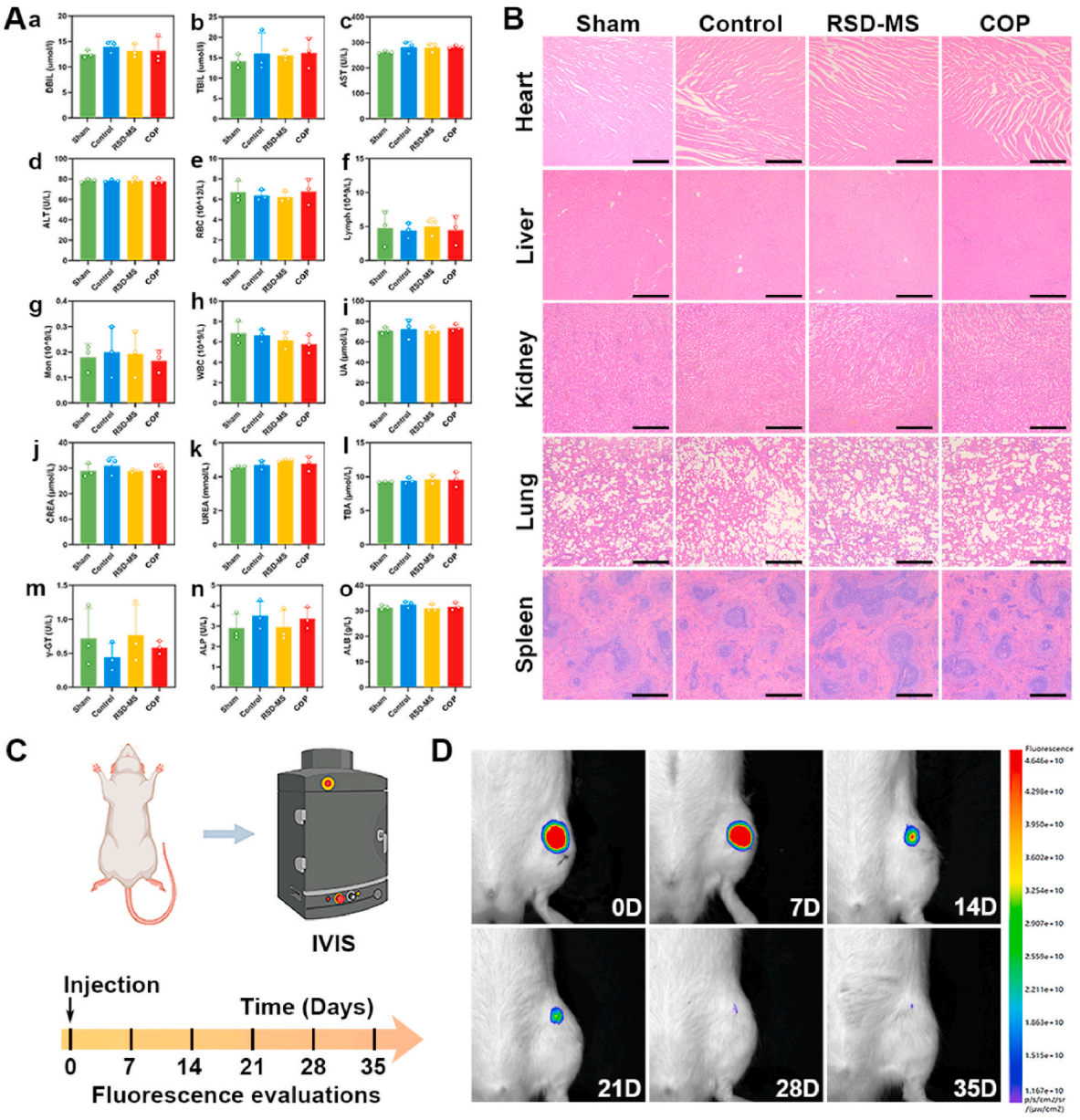

Fig. 8. (A) Blood biochemistry markers on 10 weeks. (B) The toxicity of in situ microspheres at 10 weeks (scale bars 100 μm). (C) The scheme of IVIS evaluation protocol. (D) *In vivo* degradation behavior analysis of RSD-MS.

limitations of pure DNA hydrogels.

SF-based hydrogels are emerging as promising materials in cartilage tissue engineering due to their outstanding biocompatibility, bioactivity, and mechanical properties [42,43]. Building on this, we developed a dual-network SF-DNA hydrogel with controllable mechanical strength for cartilage repair. However, conventional bulk hydrogels encounter obstacles in the fabrication of intricate functional tissues, predominantly attributable to their reduced efficiency in solute diffusion and constraints in applications at the sub-micron scale [44–46]. In an effort to surmount these challenges, our attention was directed towards hydrogel microspheres, which are engineered to augment cellular activity and differentiation potential through the facilitation of enhanced oxygen and nutrient exchange [47]. Furthermore, hydrogel microspheres exhibit superior cell delivery efficacy, particularly in the context of injectable applications [48]. Thus, their use elevates both biological performance and potential in tissue engineering. In bone tissue engineering, Ouyang et al. utilized hydrogel microspheres to construct osteo-callus organoids, achieving rapid bone defect repair within one month [49]. Additionally, Zhou et al. created bone regeneration enhancement units using BMSC-loaded microspheres, facilitating swift bone defect healing [50]. In follicle tissue engineering, Hu et al. employed gelatin methacryloyl microspheres loaded with mesenchymal and epithelial cells for rapid, large-scale hair regeneration [51]. Therefore, hydrogel microspheres hold significant potential in cartilage tissue engineering [52]. Microfluidic technology is currently considered the most advanced method for synthesizing hydrogel microspheres. This technique precisely controls droplet size and shape using microfluidic chips, producing uniformly sized and consistent hydrogel microspheres. The synthesis process is highly controllable, suitable for large-scale production, and efficient in using minute reagents. SD-MSs prepared via microfluidic technology effectively overcomes the limitations of using bulk hydrogels in constructing cartilage organoids [53].

Our research indicates that SD-MS can promote chondrogenic differentiation of BMSCs. Notably, RSD-MS exhibits a stronger capacity for chondrogenic differentiation of BMSCs. This is likely because RSD-MSs, by simulating the microenvironment of cartilage tissue through three-

dimensional high-density cell loading, enhances intercellular material exchange and signal transmission, effectively promoting BMSC growth and differentiation [53]. Additionally, transcriptomic sequencing revealed the molecular mechanisms by which RSD-MSs regulated chondrogenic differentiation of BMSCs. RSD-MS upregulates various signaling pathways related to cartilage formation, primarily integrin-mediated cell adhesion and focal adhesion pathways, and promotes GAG biosynthesis, thereby effectively inducing chondrogenic differentiation of BMSCs.

This study represents the first instance of employing SF-DNA dual-network hydrogels for the fabrication of hydrogel microspheres. *In vivo* experiments revealed that COPs demonstrated superior cartilage repair capabilities compared to RSD-MSs. Notably, the DNA network in this system displayed both excellent injectability and unique programmability. SF-DNA hydrogels not only address the challenges associated with the undefined composition and significant batch-to-batch variability of Matrigel but also hold promising prospects for future applications in 3D bioprinting. Building on prior research, we have confirmed that in SF-DNA hydrogels, DNA plays a critical role in constraining SF, thereby increasing its β-sheet content. This mechanism enables precise modulation of the hydrogel's surface rigidity, leading to customization. Appropriate stiffness, facilitated through modulation of the Wnt signaling pathway and TGF-β signaling pathway, has been shown to promote chondrogenic differentiation in BMSCs [28]. The primary focus of the research was to explore the potential of RSD-MS as a microcarrier in supporting the long-term chondrogenic differentiation of BMSCs for future use in sustaining cartilage organoid culture. In our study, hydrogel microspheres loaded with BMSCs, which have undergone 14 days of chondrogenic induction, are defined as COPs. However, these are not yet mature cartilage organoids, as they do not fully exhibit the morphology and functionalities of developed cartilage organoids. The construction of COPs indirectly confirms the potential of RSD-MSs to support long-term culture of cartilage organoids. In the future, we plan to further investigate the use of RSD-MS in cultivating mature cartilage organoids. Besides, Elvassore et al. have integrated hydrogels with bioprinting technology, allowing customization according to specific culture system requirements and desired culture durations [54].

We anticipate that by modifying DNA sequences, precise control over the properties of hydrogels can be achieved. Furthermore, integrating this approach with the 3D printing technology previously explored by our team will better fulfill the specific environmental requirements of cells during the formation of cartilage organoids [55]. This approach could potentially open a new research platform in regenerative medicine and cartilage tissue engineering, enhancing the efficiency and functionality of cartilage organoid construction for clinical applications.

4. Conclusions

In this study, we successfully by integrating photopolymerization with self-assembly through microfluidic system to develop innovative RSD-MSs for cartilage organoids construction. By modifying the surface of SD-MSs with Pep-RGDfKA, we significantly enhanced their cell adhesion capacity. The prepared RSD-MSs exhibited uniform particle size distribution, good swelling properties, and appropriate degradability. *In vitro*, RSD-MSs demonstrated excellent biocompatibility and cell adhesion, particularly in promoting BMSCs differentiation into chondrocytes. Transcriptomic analysis suggested that the chondrogenic activity of RSD-MS might be related to its influence on integrin-mediated cell adhesion and focal adhesion pathways, regulating GAG biosynthesis. To further validate these findings, we seeded BMSCs on RSD-MSs to construct COPs and studied COPs' *in vivo* cartilage repair capacity in a rat femoral cartilage defect model. AFM analysis and histological staining demonstrated significant effects of COPs in promoting cartilage regeneration.

This research provided an ideal material for constructing and long-term culturing of cartilage organoids, offering new insights into stem cell therapy. This achievement offered an innovative strategy and material selection for cartilage repair applications, demonstrating a broad range of potential applications.

5. Materials and methods

5.1. Materials

SilMA, LAP and Pep-RGDfKAC were purchased from Engineering for Life (Jiangsu, China). ssDNA was purchased from Sangon Biotech (Shanghai, China). Liquid paraffin, and Span 80 were procured from Aladdin (Shanghai, China). PBS were obtained from Corning (USA).

5.2. Preparation of SF-DNA precursor solution

As illustrated in Fig. S6, in the SD-MS developed by us, the DNA supramolecular network primarily comprises Y-scaffolds and L-linkers. The design of the ssDNA sequences that constitute this DNA supramolecular hydrogel network is detailed in Table S1. The Y-scaffold consists of three ssDNA molecules, each comprising 39 nucleotides and featuring three sticky ends of 13 nucleotides. Additionally, the L-linker is composed of two ssDNA molecules, each containing 44 nucleotides, with sticky ends of 13 nucleotides at both ends of each molecule. These ends are fully complementary to the sticky ends of the Y-scaffold. Upon thorough mixing of these ssDNA solutions, these sticky ends rapidly form the first network structure of the DNA supramolecule through crosslinking interactions. In the SD-MS, the second network is formed by photopolymerization of SilMA. SilMA is synthesized by modifying the amine residues of SF with methacrylate groups. The SF-DNA precursor solution is obtained by dissolving and mixing ssDNA (500 nmol/ml), SilMA (10 wt%), and LAP (0.25 wt%) in PBS (pH 7.4).

5.3. Preparation of SD-MSs and RSD-MSs

In this study, coaxial needle combined with microfluidic technology was employed for microsphere fabrication. The inner and outer diameters of the used coaxial needle were 340 μm and 640 μm, and 1110 μm and 1490 μm, respectively. The outlet of the coaxial needle was connected to a silicone tube to collect microspheres. During preparation, the aqueous phase (SF-DNA precursor solution) and the oil phase (5 wt% Span 80 in liquid paraffin) were injected into the inner and outer channels of the coaxial needle, respectively. Under the shear force of the oil phase, the premix was sheared into uniform droplets and flowed out of the device. To obtain uniform microspheres, the ratio of flow rates between the two phases was systematically optimized, with the aqueous phase set at 5 μl/min and the oil phase at 50 μl/min. The formed droplets were then crosslinked under UV light (365 nm wavelength, 8.0 mW cm^{-2}) to stabilize their structure. The droplets were collected in a 15 ml centrifuge tube to obtain SD-MSs. Subsequently, most of the paraffin was removed using a 30% ethanol solution in PBS. Ultimately, underwent multiple PBS washes to eliminate any remaining ethanol and paraffin.

For further surface modification, LAP (2.5 wt%) and Pep-RGDfKAC (5 wt%) were dissolved in PBS to prepare the Pep-RGDfKAC solution. Then, the Pep-RGDfKAC solution was dropwise added to the SD-MS and again crosslinked under UV illumination (365 nm, 8.0 mW cm^{-2}) for 30 s, resulting in the final RSD-MSs.

5.4. Characterization of SD-MSs and RSD-MSs

The particle sizes of SD-MSs and RSD-MSs were measured using an inverted microscope (Olympus CKX3-SLP, Japan). Subsequently, the microscope images were further analyzed using ImageJ software. The characterization of the microspheres included NMR analysis and SEM observation. Initially, the microspheres were frozen at −196 °C for 10 min, followed by a freeze-drying process for 48 h. The freeze-dried microspheres were ground into a powder and dissolved in deuterium oxide.

The composition of the microspheres was then analyzed using an NMR spectrometer (Bruker AVANCE 500 MHz, Switzerland). For SEM observation, the freeze-dried microspheres underwent gold sputter-coating utilizing a high-vacuum ion sputtering coater (Leica EM ACE600, Germany). Subsequently, the structure and morphology of the microspheres were observed using a cold field emission SEM (JSM-7500F, JEOL Ltd, Japan). The pore size of the lyophilized hydrogels was measured utilizing ImageJ software, analyzing SEM imagery. The swelling ratio of the microspheres was ascertained through a gravimetric approach, adhering to a pre-defined experimental procedure [56]. The initial dry weight (M0) of the microspheres and their weight after swelling in PBS solution at room temperature (M1) were measured. The swelling ratio was calculated utilizing the formula: Swelling ratio = (M1/M0) × 100%. For the degradation experiments of SD-MSs and RSD-MSs, Protease K, a widely used enzyme for degrading silk materials, was employed. The freeze-dried microspheres were first weighed (M0), then immersed in PBS (pH 7.4) and Protease K solution (5U/mL in 10 mmol/L PBS buffer) at 37 °C on a shaker. The PBS and Protease K solution were replaced every 24 h. At specified intervals (1, 3, 7, 14, 21, 28 days), the microspheres were reweighed (M1). The weight residual rate of the hydrogel was calculated using the formula: Weight residual rate = (M1/M0) × 100%.

5.5. In Vitro cell culture

BMSCs from rats were obtained from a cell bank (Shanghai, China) for subsequent *in vitro* experiments. The cells were cultured in Minimum Essential Medium α (MEMα, Corning, USA) containing 10% Fetal Bovine Serum (FBS, Sigma, USA) and 1% Penicillin-Streptomycin (Gibco, USA). The culture environment was maintained at 37 °C with 5% CO_2. The culture medium was replaced every two days, and third-generation BMSCs were used for cell experiments.

5.5.1. Cytotoxicity and cell adhesion assay

To study the activity of microspheres cocultured with BMSCs, a 24-well transwell plate (pore size 0.4 μm, Corning, USA) coculture system was used [57]. The SD-MSs and RSD-MSs were sterilized under UV light for 2 h, followed by a live/dead cell staining method to assess their cytotoxicity. BMSCs (5×10^4) were seeded in the lower chamber of the transwell plate, and 100 μl sterilized microspheres were deposited in the upper chamber. After coculture for 1, 3, and 5 days, the cells were incubated with the Calcein AM/PI double staining kit for 30 min and observed under a fluorescence microscope for cell viability assessment. Additionally, the impact of microspheres on BMSCs proliferation was assessed utilizing a Cell Counting Kit-8 (CCK-8, Beyotime, China) colorimetric assay. BMSCs (2×10^4) were cultured in the lower chamber of the transwell plate, with 100 μl of microspheres in the upper chamber. On days 1, 3, and 5 of cell culture, CCK-8 solution was introduced to each lower chamber of the transwell plate, incubated for 2 h at 37 °C, 5% CO_2, and the absorbance of the supernatant was measured at 450 nm utilizing a multi-mode microplate reader to quantitatively assess BMSCs proliferation.

To further proved the cell adhesion capability of RSD-MSs, BMSCs were cocultured with RSD-MSs in low-adhesion culture dishes (Nest Biotech, China). On days 1, 3, 7and 14 after cell seeding, staining was performed using TRITC Phalloidin (Solarbio, China) and DAPI (Beyotime, China) following standard protocols, and cell adhesion and proliferation on the microspheres were observed. 3D fluorescence images were acquired using a confocal laser scanning microscope (Olympus FV3000, Japan). And fluorescence images were acquired using an inverted microscope (Olympus CKX3-SLP, Japan). Furthermore, the proliferation of BMSCs covered on microspheres was assessed using the CCK-8 (Beyotime, China) colorimetric assay.

5.5.2. Chondrogenic differentiation

Similarly, we utilized a transwell plate coculture system, culturing BMSCs (2×10^4) in the lower chamber of the transwell plate, with 100 μl of microspheres deposited in the upper chamber, alongside an equal number (2×10^4) of BMSCs. Cells were incubated in a chondrogenic induction medium comprising 1 mM sodium pyruvate (Sigma, USA), 10 ng/ml Transforming Growth Factor-β3 (Meilunbio, China), 0.1 μM dexamethasone (Sigma, USA), 1% ITS premix (Oricellbio, China), and 1 μM ascorbic acid-2-phosphate (Sigma, USA). The medium was refreshed every 2 days. On days 3, 7, and 14 of culture, cells were fixed using 4% paraformaldehyde solution and then stained with 1% Alcian Blue (pH = 2.5). Post-staining, cells were washed with 6 M guanidine HCl to elute the dye, and the absorbance of the eluted dye solution was measured at 630 nm utilizing a multi-mode microplate reader for quantitative analysis.

Total protein from the cell-microsphere constructs was extracted using high-efficiency RIPA tissue/cell lysis solution (Beyotime, China), and the content of Col II was determined using a rabbit Col II assay kit (Cloud-Clone, China) following the manufacturer's protocol [58]. 10 μL of digested sample was mixed with 100 μL of DMMB (Sigma, USA) and incubated at 37 °C for 30 min for staining, followed by measuring optical density (OD) at 525 nm. GAG content was determined using shark cartilage chondroitin sulfate-6 (Sigma, USA) as a standard substance provided. With the same method applied to the experimental materials to exclude the influence of material components on the results.

To investigate the impact of hydrogels on chondrogenic differentiation of BMSCs, qRT-PCR technology was utilized to detect the expression levels of cartilage-specific genes (Sox9, ACAN, and Col II), fibrotic genes (Col I), and hypertrophic genes (Col X) in BMSCs with different microspheres. Primer sequences for relevant genes are listed in Table S2. Proteins were extracted using RIPA lysis solution containing PMSF, protease inhibitors, and phosphatase inhibitors. After SDS-PAGE electrophoresis, target proteins were transferred onto PVDF membranes. They were first blocked with bovine serum albumin (Beyotime, China) for 1 h to prevent non-specific protein binding, followed by an overnight incubation at 4 °C with rabbit anti- Col II, anti-Sox9, and *anti*-ACAN antibodies (1:1000, Abcam, US). Subsequently, they were incubated for 2 h with Goat Anti-Rabbit IgG H&L secondary antibody (1:5000, Abcam, US) at room temperature and detected using an enhanced chemiluminescence (ECL) system. Experimental samples were incubated for 2 h with Goat Anti-Rabbit IgG H&L (1:5000, Abcam, USA) at room temperature and detected with the primary antibody. After this step, the signal was detected using an ECL. Finally, for quantitative analysis of the results, ImageJ software was used for further quantification, accurately assessing the expression levels of the target proteins.

5.6. Transcriptomic analysis (mRNA-seq)

BMSCs samples, cocultured for 14 days on RSD-MSs and designated as the RSD-MS group, were collected. Total RNA from these cell samples was extracted using TRIzol reagent, and corresponding RNA libraries were constructed, followed by high-throughput sequencing (OE Biotech Co., Ltd., China). For sequencing data analysis, DESeq software was utilized to identify DEGs. In this study, genes with a *P*-value less than 0.05 and a fold change greater than 2 or less than 0.5 were considered significantly differentially expressed. Additionally, for in-depth bioinformatics analysis, GO enrichment analysis, KEGG pathway enrichment analysis, and GSEA were employed.

5.7. In Vivo cartilage repair of microspheres

In this study, male Sprague-Dawley (SD) rats (6 weeks old, weighing approximately 150g) were obtained from Changzhou Cavens Laboratory Animal Co., Ltd. All animal experimental procedures were strictly conducted in accordance with the established guidelines for animal experiments and had received approval from the Animal Ethics Committee of Shanghai University. The rats were distinctly divided into four groups: Sham group, Control group, SD-MS group, and COP group.

Following general anesthesia (using Sodium Pentobarbital at a dosage of 80 mg/kg), a cartilage defect model with a diameter of 2 mm and a depth of 1.5 mm was created in the central region of the intercondylar notch in SD rats. The therapeutic microsphere suspension was prepared by mixing PBS with RSD-MSs or COPs in a volume ratio of 2:1. Subsequently, approximately 20 μL of microsphere suspension was injected into the defect site using a syringe, followed by the application of fibrin glue at the site of the defect for fixation. The knee joint capsule and skin were then sutured and disinfected, and all rats were provided with standardized care. At 5 and 10 weeks post-operation, the rats were euthanized, and samples of their femurs, hearts, livers, spleens, lungs, kidneys, and abdominal aorta blood were collected for subsequent analysis. Additionally, at 5 and 10 weeks post-operation, macroscopic observations of the treatment effect on the articular cartilage of the femoral condyles in SD rats were conducted. All rat femur samples were soaked in 4% formalin for 48 h to fix the tissue. To assess the surface roughness of the regenerated cartilage area, AFM analysis was performed using the Bruker Dimension ICOM system. All samples (n = 5) underwent AFM assessment using Bruker Dimension ICON. Subsequently, the femoral condyles were decalcified for 6 weeks and embedded in paraffin at appropriate orientations. Following embedding, the samples were dehydrated through an ethanol gradient and sectioned into 10 μm thick slices. Subsequently, the sections were subjected to staining with Safranin O/Fast Green and H&E. And the expression of ACAN and Col II in the defect area was detected using immunohistochemical methods. Subsequently, for quantitative analysis of the immunohistochemical results, we employed ImageJ software for further quantification, thereby accurately assessing the expression levels of the target protein. At 10 weeks post-operation, samples from key organs (heart, liver, kidney, spleen, lung) were collected for pathological staining, and routine blood and liver and kidney function tests were performed from abdominal aorta blood samples to evaluate the biocompatibility of the microspheres.

5.8. In Vivo degradation capability of microspheres

Initially, RSD-MSs were prepared. For fluorescent labeling, these microspheres were immersed in a Sulfo-Cy5.5 NHS ester solution (DuoFluor, China) for 1 h to label them with Cy5.5. The microspheres were then washed three times to remove excess fluorescent markers, thereby constructing Cy5.5-labeled microspheres. PBS was combined with Cy5.5-labeled RSD-MSs at a volume ratio of 2:1 to formulate a microsphere suspension. This suspension of Cy5.5-labeled RSD-MS microspheres was then injected into the knee joint cavities of SD rats in a volume of 20 μL. An *in vivo* imaging system (IVIS, Biolight Biotechnology, AniView100, China) was used to assess the retention of the microspheres *in vivo*. Fluorescence intensity measurements were conducted at 0, 1, 2, 3, 4, and 5 weeks. The excitation/emission wavelengths were set at 675/740 nm, and the relative fluorescence intensity at each designated time point was adjusted relative to week 0.

5.9. Statistical analysis

All experimental data were derived from at least three independent experiments and are expressed as mean ± standard deviation. Comparisons between groups were made using a *t*-test, and comparisons among multiple groups were conducted using one-way analysis of variance (ANOVA). A threshold of statistical significance was set at a p-value of less than 0.05.

Data availability

Data supporting the findings of this study can be obtained from the corresponding author upon request.

Ethics approval and consent to participate

All animal experimental procedures were strictly conducted in accordance with the established guidelines for animal experiments and had received approval from the Animal Ethics Committee of Shanghai University (YS-2023-032).

CRediT authorship contribution statement

Congyi Shen: Writing – original draft, Resources, Methodology. **Jian Wang:** Methodology, Resources. **Guangfeng Li:** Conceptualization. **Shuyue Hao:** Resources, Writing – original draft. **Yan Wu:** Methodology. **Peiran Song:** Visualization. **Yafei Han:** Resources, Software. **Mengmeng Li:** Software. **Guangchao Wang:** Methodology. **Ke Xu:** Software, Formal analysis. **Hao Zhang:** Investigation. **Xiaoxiang Ren:** Resources, Data curation. **Yingying Jing:** Supervision, Writing – review & editing. **Ru Yang:** Resources, Writing – review & editing. **Zhen Geng:** Writing – review & editing, Supervision, Funding acquisition, Conceptualization. **Jiacan Su:** Writing – review & editing, Supervision, Project administration, Funding acquisition, Conceptualization.

Declaration of competing interest

The authors declare that they have no known competing financial interests or personal relationships that could have appeared to influence the work reported in this paper.

Acknowledgements

This work was supported by the National Key Research and Development Program of China (No. 2022YFB3804300), Integrated Project of Major Research Plan of National Natural Science Foundation of China (92249303), Key Project of the National Natural Science Foundation of China (82230071), National Natural Science Foundation of China (32101084).

Appendix A. Supplementary data

Supplementary data to this article can be found online at https://doi.org/10.1016/j.bioactmat.2024.02.016.

References

[1] Z. Liu, Y. Zhuang, L. Fang, C. Yuan, X. Wang, K. Lin, Breakthrough of extracellular vesicles in pathogenesis, diagnosis and treatment of osteoarthritis, Bioact. Mater. 22 (2023) 423–452.
[2] D.J. Hunter, S. Bierma-Zeinstra, Osteoarthritis. The Lancet 393 (10182) (2019) 1745–1759.
[3] R.F. Loeser, S.R. Goldring, C.R. Scanzello, B. M, Goldring. Osteoarthritis: a disease of the joint as an organ, Arthritis Rheumatol. 64 (6) (2012) 1697–1707.
[4] D.J. Hunter, D. Schofield, E. Callander, The individual and socioeconomic impact of osteoarthritis, Nat. Rev. Rheumatol. 10 (7) (2014) 437–441.
[5] H. Long, Q. Liu, H. Yin, K. Wang, N. Diao, Y. Zhang, J. Lin, A. Guo, Prevalence trends of site-specific osteoarthritis from 1990 to 2019: findings from the global burden of disease study 2019, Arthritis Rheumatol. 74 (7) (2022) 1172–1183.
[6] J.D. Li, H. Zhang, Y.F. Han, Y. Hu, Z. Geng, J.C. Su, Targeted and responsive biomaterials in osteoarthritis, Theranostics 13 (3) (2023) 931–954.
[7] Z. Geng, S. Sang, S. Wang, F. Meng, Z. Li, S. Zhu, Z. Cui, Y. Jing, C. Wang, J. Su, Optimizing the strontium content to achieve an ideal osseointegration through balancing apatite-forming ability and osteogenic activity, Bioact. Mater. 133 (112647) (2022).
[8] D.J. Du, P.C. Hsu, Z.Z. Zhu, C.Q. Zhang, Current surgical options and innovation for repairing articular cartilage defects in the femoral head, Journal of Orthopaedic Translation 21 (2020) 122–128.
[9] Y. Zhuang, S. Jiang, C. Yuan, K. Lin, The potential therapeutic role of extracellular vesicles in osteoarthritis, Front. Bioeng. Biotechnol. (2022) 10.
[10] H. Kwon, W.E. Brown, C.A. Lee, D. Wang, N. Paschos, J.C. Hu, K.A. Athanasiou, Surgical and tissue engineering strategies for articular cartilage and meniscus repair, Nat. Rev. Rheumatol. 15 (9) (2019) 550–570.
[11] E.A. Makris, A.H. Gomoll, K.N. Malizos, J.C. Hu, K.A. Athanasiou, Repair and tissue engineering techniques for articular cartilage, Nat. Rev. Rheumatol. 11 (1) (2015) 21–34.

[12] W.Y.W. Lee, B. Wang, Cartilage repair by mesenchymal stem cells: clinical trial update and perspectives, Journal of Orthopaedic Translation 9 (76) (2017) 88.
[13] M.A. Lancaster, J.A. Knoblich, Organogenesis in a dish: modeling development and disease using organoid technologies, Science 345 (6194) (2014) 1247125.
[14] T. Takebe, J.M. Wells, Organoids by design, Science 364 (6444) (2019) 956–959.
[15] M. Hofer, M.P. Lutolf, Engineering organoids, Nat. Rev. Mater. 6 (5) (2021) 402–420.
[16] Y. Hu, H. Zhang, S.C. Wang, L.H. Cao, F.J. Zhou, Y.Y. Jing, J.C. Su, Bone/cartilage organoid on-chip: construction strategy and application, Bioact. Mater. 25 (29–41) (2023).
[17] H. Zhang, S.L. Wu, W.K. Chen, Y. Hu, Z. Geng, J.C. Su, Bone/cartilage targeted hydrogel: strategies and applications, Bioact. Mater. 23 (2023) 156–169.
[18] Y. Wang, Y. Chen, Y. Wei, Osteoarthritis animal models for biomaterial-assisted osteochondral regeneration, Biomaterials translational 3 (4) (2022) 264–279.
[19] M. Tamaddon, H. Gilja, L. Wang, J.M. Oliveira, X. Sun, R. Tan, C. Liu, Osteochondral scaffolds for early treatment of cartilage defects in osteoarthritic joints: from bench to clinic, Biomaterials translational 1 (1) (2020) 3–17.
[20] M. Sahranavard, S. Sarkari, S. Safavi, F. Ghorbani, Three-dimensional bio-printing of decellularized extracellular matrix-based bio-inks for cartilage regeneration: a systematic review, Biomaterials translational 3 (2) (2022) 105–115.
[21] J.H. Xu, S. Fang, S.X. Deng, H.J. Li, X.N. Lin, Y.H. Huang, S.M. Chung, Y.S. Shu, Z. C. Shao, Generation of neural organoids for spinal-cord regeneration via the direct reprogramming of human astrocytes, Nat. Biomed. Eng. 7 (3) (2023) 253.
[22] Z. Zhang, S. Gao, Y.N. Hu, X. Chen, C. Cheng, X.L. Fu, S.S. Zhang, X.L. Wang, Y. W. Che, C. Zhang, R.J. Chai, Ti3C2TxMXene composite 3D hydrogel potentiates mTOR signaling to promote the generation of functional hair cells in cochlea organoids, Adv. Sci. 9 (32) (2022).
[23] H. Zhang, S. Wu, W. Chen, Y. Hu, Z. Geng, J. Su, Bone/cartilage targeted hydrogel: strategies and applications, Bioact. Mater. 23 (2023) 156–169.
[24] P. Song, D. Ye, X. Zuo, J. Li, J. Wang, H. Liu, M.T. Hwang, J. Chao, S. Su, L. Wang, J. Shi, L. Wang, W. Huang, R. Lal, C. Fan, DNA hydrogel with aptamer-toehold-based recognition, cloaking, and decloaking of circulating tumor cells for live cell analysis, Nano Lett. 17 (9) (2017) 5193–5198.
[25] J. Shi, Z. Shi, Y. Dong, F. Wu, D. Liu, Responsive DNA-based supramolecular hydrogels, ACS Appl. Bio Mater. 3 (5) (2020) 2827–2837.
[26] Y. Shao, H. Jia, T. Cao, D. Liu, Supramolecular hydrogels based on DNA self-assembly, Accounts Chem. Res. 50 (4) (2017) 659–668.
[27] J. Tang, C. Yao, Z. Gu, S. Jung, D. Luo, D. Yang, Super-soft and super-elastic DNA robot with magnetically driven navigational locomotion for cell delivery in confined space, Angew Chem. Int. Ed. Engl. 59 (6) (2020) 2490–2495.
[28] Z.Y. Zhou, P.R. Song, Y. Wu, M.M. Wang, C.Y. Shen, Z.X. Ma, X.X. Ren, X.H. Wang, X. Chen, Y. Hu, Z.H. Li, Q. Zhang, M.M. Li, Z. Geng, J.C. Su, Dual-network DNA-silk fibroin hydrogels with controllable surface rigidity for regulating chondrogenic differentiation, Mater. Horiz. (2024). In Press.
[29] Q. He, J. Zhang, Y. Liao, E.V. Alakpa, V. Bunpetch, J. Zhang, H. Ouyang, Current advances in microsphere based cell culture and tissue engineering, Biotechnol. Adv. 39 (2020).
[30] Q. Gao, L. Wang, S. Wang, B. Huang, Y. Jing, J. Su, Bone marrow mesenchymal stromal cells: identification, classification, and differentiation, Front. Cell Dev. Biol. 9 (787118) (2021).
[31] A. Saraswathibhatla, D. Indana, O. Chaudhuri, Cell-extracellular matrix mechanotransduction in 3D, Nat. Rev. Mol. Cell Biol. 24 (7) (2023) 495–516.
[32] J. Wu, L.W. Fu, Z.E. Yan, Y. Yang, H. Yin, P.X. Li, X. Yuan, Z.A. Ding, T. Kang, Z. Tian, Z.Y. Liao, G.Z. Tian, C. Ning, Y.G. Li, X. Sui, M.X. Chen, S.Y. Liu, Q.Y. Guo, Hierarchical porous ECM scaffolds incorporating GDF-5 fabricated by cryogenic 3D printing to promote articular cartilage regeneration, Biomater. Res. 27 (1) (2023).
[33] S. Wu, H. Zhang, S. Wang, J. Sun, Y. Hu, H. Liu, J. Liu, X. Chen, F. Zhou, L. Bai, X. Wang, J. Su, Ultrasound-triggered in situ gelation with ROS-controlled drug release for cartilage repair, Mater. Horiz. 10 (9) (2023) 3507–3522.
[34] S. Wu, X. Wu, X. Wang, J. Su, Hydrogels for bone organoid construction: from a materiobiological perspective, J. Mater. Sci. Technol. 136 (21–31) (2023).
[35] K. Abe, A. Yamashita, M. Morioka, N. Horike, Y. Takei, S. Koyamatsu, K. Okita, S. Matsuda, N. Tsumaki, Engraftment of allogeneic iPS cell-derived cartilage organoid in a primate model of articular cartilage defect, Nat. Commun. 14 (1) (2023) 804.
[36] Y. Zhang, G.F. Li, J. Wang, F.J. Zhou, X.X. Ren, J.C. Su, Small Joint Organoids 3D Bioprinting: Construction Strategy and Application, Small, 2023.
[37] Z. Yang, B. Wang, W. Liu, X. Li, K. Liang, Z. Fan, J.J. Li, Y. Niu, Z. He, H. Li, D. Wang, J. Lin, Y. Du, J. Lin, D. Xing, In situ self-assembled organoid for osteochondral tissue regeneration with dual functional units, Bioact. Mater. 27 (2023) 200–215.
[38] D. Xing, W. Liu, J.J. Li, L. Liu, A. Guo, B. Wang, H. Yu, Y. Zhao, Y. Chen, Z. You, C. Lyu, W. Li, A. Liu, Y. Du, J. Lin, Engineering 3D functional tissue constructs using self-assembling cell-laden microniches, Acta Biomater. 114 (2020) 170–182.
[39] Z. Xiahou, Y. She, J. Zhang, Y. Qin, G. Li, L. Zhang, H. Fang, K. Zhang, C. Chen, J. Yin, Designer hydrogel with intelligently switchable stem-cell contact for incubating cartilaginous microtissues, ACS Appl. Mater. Interfaces 12 (36) (2020) 40163–40175.
[40] Y.X. Xu, Q.O. Wu, Y.Q. Sun, H. Bai, G.Q. Shi, Three-dimensional self-assembly of graphene oxide and DNA into multifunctional hydrogels, ACS Nano 4 (12) (2010) 7358–7362.
[41] Y.H. Peng, S.K. Hsiao, K. Gupta, A. Ruland, G.K. Auernhammer, M.F. Maitz, S. Boye, J. Lattner, C. Gerri, A. Honigmann, C. Werner, E. Krieg, Dynamic matrices with DNA-encoded viscoelasticity for cell and organoid culture, Nat. Nanotechnol. (2023).
[42] X. Xue, H. Zhang, H. Liu, S. Wang, J. Li, Q. Zhou, X. Chen, X. Ren, Y. Jing, Y. Deng, Z. Geng, X. Wang, J. Su, Rational design of multifunctional CuS nanoparticle-PEG composite soft hydrogel-coated 3D hard polycaprolactone scaffolds for efficient bone regeneration, Adv. Funct. Mater. 32 (33) (2022).
[43] Z. Zhou, J. Cui, S. Wu, Z. Geng, J. Su, Silk fibroin-based biomaterials for cartilage/osteochondral repair, Theranostics 12 (11) (2022) 5103–5124.
[44] L. Xie, J. Zhang, H. Sun, Z. Chen, W. Teng, X. Chai, C. Wang, X. Yang, Y. Li, S. Xu, Z. Gou, Z. Ye, Mechanically strong porous bioceramic tubes facilitate large segmental bone defect repair by providing long-term structurally stability and promoting osteogenesis, Engineered Regeneration 5 (1) (2024) 1–10.
[45] C. Huang, Q. Ye, J. Dong, L. Li, M. Wang, Y. Zhang, Y. Zhang, X. Wang, P. Wang, Q. Jiang, Biofabrication of natural Au/bacterial cellulose hydrogel for bone tissue regeneration via in-situ fermentation, Smart Materials in Medicine 4 (1–14) (2023).
[46] X. Yu, X. Wang, D. Li, R. Sheng, Y. Qian, R. Zhu, X. Wang, K. Lin, Mechanically reinforced injectable bioactive nanocomposite hydrogels for in-situ bone regeneration, Chem. Eng. J. (2022) 433.
[47] X. Li, X. Li, J. Yang, J. Lin, Y. Zhu, X. Xu, W. Cui, Living and injectable porous hydrogel microsphere with paracrine activity for cartilage regeneration, Small 19 (17) (2023) e2207211.
[48] T. Wang, Y. Li, J. Liu, Y. Fang, W. Guo, Y. Liu, X. Li, G. Li, X. Wang, Z. Zheng, X. Wang, D.L. Kaplan, Intraarticularly injectable silk hydrogel microspheres with enhanced mechanical and structural stability to attenuate osteoarthritis, Biomaterials (121611) (2022) 286.
[49] C. Xie, R. Liang, J. Ye, Z. Peng, H. Sun, Q. Zhu, X. Shen, Y. Hong, H. Wu, W. Sun, X. Yao, J. Li, S. Zhang, X. Zhang, H. Ouyang, High-efficient engineering of osteo-callus organoids for rapid bone regeneration within one month, Biomaterials (121741) (2022) 288.
[50] Z. Cai, X. Liu, M. Hu, Y. Meng, J. Zhao, Y. Tan, X. Luo, C. Wang, J. Ma, Z. Sun, Y. Jiang, B. Lu, R. Gao, F. Chen, X. Zhou, In situ enzymatic reaction generates magnesium-based mineralized microspheres with superior bioactivity for enhanced bone regeneration, Adv. Healthcare Mater. 12 (24) (2023) e2300727.
[51] J. Huang, D. Fu, X. Wu, Y. Li, B. Zheng, Z. Liu, Y. Zhou, Y. Gan, Y. Miao, Z. Hu, One-step generation of core-shell biomimetic microspheres encapsulating double-layer cells using microfluidics for hair regeneration, Biofabrication 15 (2) (2023).
[52] S.D. Liao, H.Y. Meng, J.K. Li, J. Zhao, Y.C. Xu, A.Y. Wang, W.J. Xu, J. Peng, S.B. Lu, Potential and recent advances of microcarriers in repairing cartilage defects, Journal of Orthopaedic Translation 27 (2021) 101–109.
[53] Q. Pan, W.X. Su, Y.C. Yao, Progress in microsphere-based scaffolds in bone/cartilage tissue engineering, Biomed. Mater. 18 (6) (2023).
[54] A. Urciuolo, G.G. Giobbe, Y. Dong, F. Michielin, L. Brandolino, M. Magnussen, O. Gagliano, G. Selmin, V. Scattolini, P. Raffa, P. Caccin, S. Shibuya, D. Scaglioni, X. Wang, J. Qu, M. Nikolic, M. Montagner, G.L. Galea, H. Clevers, M. Giomo, P. De Coppi, N. Elvassore, Hydrogel-in-hydrogel live bioprinting for guidance and control of organoids and organotypic cultures, Nat. Commun. 14 (1) (2023) 3128.
[55] X. Ren, J. Wang, Y. Wu, Y. Zhang, J. Zhang, L. Bai, J. Liu, G. Li, P. Song, Z. Shi, J. Su, One-pot synthesis of hydroxyapatite hybrid bioinks for digital light processing 3D printing in bone regeneration, J. Mater. Sci. Technol. 188 (2024) 84–97.
[56] W.Z. Jiang, X.T. Xiang, M.K. Song, J.L. Shen, Z.J. Shi, W.H. Huang, H. Liu, An all-silk-derived bilayer hydrogel for osteochondral tissue engineering, Materials Today Bio 17 (2022).
[57] J. Lin, L. Chen, J. Yang, X. Li, J. Wang, Y. Zhu, X. Xu, W. Cui, Injectable double positively charged hydrogel microspheres for targeting-penetration-phagocytosis, Small 18 (40) (2022) e2202156.
[58] Y.R. Chen, X. Yan, F.Z. Yuan, L. Lin, S.J. Wang, J. Ye, J.Y. Zhang, M. Yang, D. C. Wu, X. Wang, J.K. Yu, Kartogenin-conjugated double-network hydrogel combined with stem cell transplantation and tracing for cartilage repair, Adv. Sci. 9 (35) (2022) e2105571.